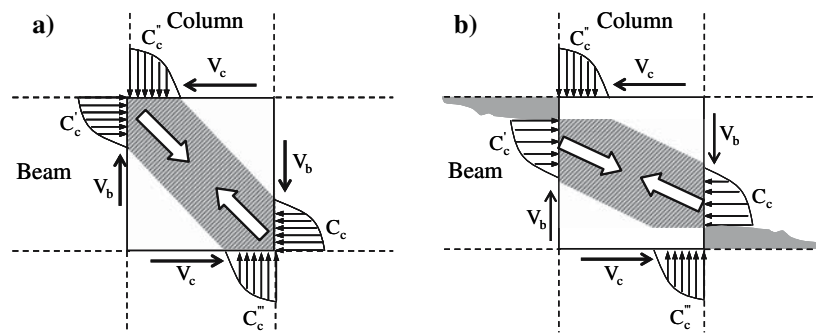


**Fig. 15** Change in strut geometry after spalling of beam section. (a) Concrete diagonal strut. (b) Concrete strut after spalling of beam section



column joint in substandard existing frame may perform in a moderately ductile flexural mode if the size of column is large. The research is needed to investigate the size and stress condition of column that can serve to prioritize substandard RC buildings for seismic rehabilitation.

2. The provision of substantial horizontal joint reinforcement may not prevent joint shear failure even though the bond was not lost. The ACI minimum joint shear reinforcement may thus not be adequate for moderately ductile joint performance.
3. Within the scope of the test program, the complete un-bonding of bar within the joint was found to cause only a slight reduction in column shear. In addition, un-bonding the bar may reduce the joint damage and avoid the joint shear failure, which is favored in terms of post-earthquake repair. In this regards, the un-bonding can perhaps be considered for new construction. Further research is needed to clarify the behavior of joint with un-bonded bars.
4. The development of tensile strain in steel bars was related to the failure mode and was not dependent on bond anchorage in joint core. When the failure occurred in beam, high tensile strain was developed in steel but when the failure occurred in joint, the strain in steel was reduced. The reinforcement could develop high plastic strain even without bond in the joint. The anchorage zone may be found along the bar outside the joint region.
5. In specimen with un-bonded bar, the loss of spalled concrete section may reduce the joint shear force by moving down the compression stress block. The compression resultant on

opposite faces then became aligned with flatter inclination. The capacity of compression strut thus increases, which prevents joint shear failure and reduces joint damage.

In view of the significance of the problem, further research works related to anchorage bond, joint shear stress and horizontal joint reinforcements are highly needed to strengthen the above conclusions and to realize the implementation of the findings in this paper. The condition of existing stress and strain due to gravity load on beam should also be studied.

**Acknowledgements** The authors are very grateful to Thailand Research Fund (TRF) for providing the research fund RMU4880022 to carry out the research.

## References

1. Paulay T, Park R, Priesley MJN (1978) Reinforced concrete beam–column joints under seismic actions. *ACI Struct J* 75:585–593
2. Bonacci J, Pantazopoulou S (1993) Parametric investigation of joint mechanics. *ACI Struct J* 90(1):61–71
3. Shiohara H (2001) New model for shear failure of RC interior beam–column connections. *J Struct Eng ASCE* 127:152–160
4. Kitayama K, Otani S, Aoyama H (1991) Development of design criteria for RC interior beam–column joints. *ACI SP-123 Design of beam–column joints for seismic resistance*. American Concrete Institute, Michigan, pp 97–123
5. Standards New Zealand (1995) *Design of concrete structure*. (NZS 3101:1995). Wellington, New Zealand
6. ACI Committee 318 (2005) *Building code requirements for structural concrete and commentary*. Michigan, USA
7. El-Attar AG, White RN, Gergeley P (1997) Behavior of gravity load designed reinforced concrete buildings subjected to earthquakes. *ACI Struct J* 94(2):133–145
8. Hakuto S, Park R, Tanaka H (2000) Seismic load tests on interior and exterior beam–column joints with substandard reinforcing details. *ACI Struct J* 97(1):11–25
9. Aycardi LE, Mander JB, Reinhorn AM (1994) Seismic resistance of reinforced concrete frame structures designed

- only for gravity loads: experimental performance of sub-assemblages. *ACI Struct J* 91(5):552–563
10. Warnichai P (2004) Development of seismic design requirements for buildings in Bangkok against the effects of distant large earthquakes. Proceedings of the 13th world conference on earthquake engineering, Vancouver
  11. Chaimahawan P, Pimanmas A (2006) Seismic vulnerability of existing reinforced concrete buildings in Bangkok. Proceedings of the 5th international symposium on new technologies for urban safety of megacities in Asia (US-MCA), Thailand
  12. Kato B (1979) Mechanical properties of steel under load cycles idealizing seismic actions. Proceedings of AICAP-CEB symposium on structural concrete under severe seismic actions, Rome, Bulletin D' Information No. 131, pp 7–27

## Seismic retrofit of substandard beam-column joint by planar joint expansion

Preeda Chaimahawan · Amorn Pimanmas

Received: 1 June 2007 / Accepted: 15 May 2008  
© RILEM 2008

**Abstract** A seismic retrofit technique for existing reinforced concrete beam-column connections using planar joint expansion is proposed. The method is based on a two-dimensional expansion of beam-column joint using cast in-situ concrete and dowel bars. The method is economical and architecturally acceptable. Three half-scale sub-standard beam-column specimens were tested under quasi-static cyclic loading. One was control specimen and the other two were retrofitted specimens with triangular and square joint expansion. According to test results, the control specimen showed brittle joint shear failure while retrofitted specimens showed beam flexural failure. The strength, stiffness, energy dissipation and ductility of retrofitted specimens were greatly improved. The planar joint expansion is effective to reduce joint shear stress and improve anchorage bond of beam bar within the joint. The plastic hinge formation can be moved away from column face, thus preventing joint shear failure. The triangular and square expansions perform almost equally well. The construction joints formed at the interfaces between specimen and joint expansion do not produce an adverse effect in cyclic behavior.

**Keywords** Substandard beam-column connection · Joint shear failure · Seismic retrofit · Planar joint expansion · Plastic hinge

### Notations

$b_b$	Beam width
$b_c$	Column width
$d_b$	Diameter of longitudinal beam bar
$f'_c$	Cylindrical compressive strength of concrete
$f_y$	Yield strength of steel
$h_b$	Beam depth
$h_c$	Column depth
$h_h$	Dimension of joint expansion along beam
$h_v$	Dimension of joint expansion along column
$b_p$	Width of joint expansion
$M_{nb}$	Moment capacity of beam
$M_{nc}$	Moment capacity of column
$T$	Tension force
$T'$	Tension force on opposite section
$V_c$	Column shear force
$V_{cj}$	Column shear force transmitted in joint core
$V_{jh}$	Horizontal joint shear force
$V_n$	Joint shear capacity
$v_{jh}$	Joint shear stress
$\rho_s$	Volumetric ratio of joint reinforcement
$BI$	Bond index
$\gamma$	Joint shear deformation
$a$	Horizontal distance of measuring point
$b$	Vertical distance of measuring point

P. Chaimahawan · A. Pimanmas (✉)  
School of Civil Engineering and Technology,  
Sirindhorn International Institute of Technology,  
Thammasat University, Patumthani 12121, Thailand  
e-mail: amorn@siit.tu.ac.th



- $\Delta_1$  Displacement measured from transducer 1  
 $\Delta_2$  Displacement measured from transducer 2

## 1 Introduction

In many regions of the world, there are many existing reinforced concrete buildings not designed for seismic actions. In particular, buildings constructed before 1970 are likely to possess non-ductile reinforcement details owing to older seismic design codes that do not incorporate capacity design concept [1]. Moreover, many buildings in zones of low seismicity, such as the eastern and central parts of the United States [2–4] and Southeast Asian countries like Thailand, Singapore and Malaysia, are normally designed for gravity load only. The design of buildings usually follows the American Concrete Building code (ACI) in Thailand and British code (BS) in Singapore and Malaysia.

Recent seismic studies [5] have indicated that damaging earthquakes can occur in these regions. Recently, the 2004 Sumatra earthquake recorded at a magnitude of 9.3 on Richter Scale has caused violent shaking of many buildings in Bangkok though the epicenter is more than 800 km far away. The quake has raised public concern on seismic safety of buildings. The seismic evaluation program of existing buildings in Bangkok has revealed seismic deficiencies of reinforced concrete buildings [6]. Interior beam-column connection is identified as one of the most critical components. In many cases, the failure of beam-column joints can lead to the entire collapse of buildings.

The common failure modes of beam-column joint are joint shear failure and anchorage failure of longitudinal beam bars passing through the joint [7, 8]. In order to mitigate seismic hazard in existing structures, researches on seismic rehabilitation of existing structures have received considerable attention during the past two decades. Several retrofitting methods for beam-column joints have been proposed. Concrete jacketing of beam-column joint is one of the common techniques [9]. However, this method produces protruding parts of jacketing in floor space which is of architectural limitation for practical use.

Strengthening joint shear resistance by using steel plates, rods, and jackets has been tested by Beres

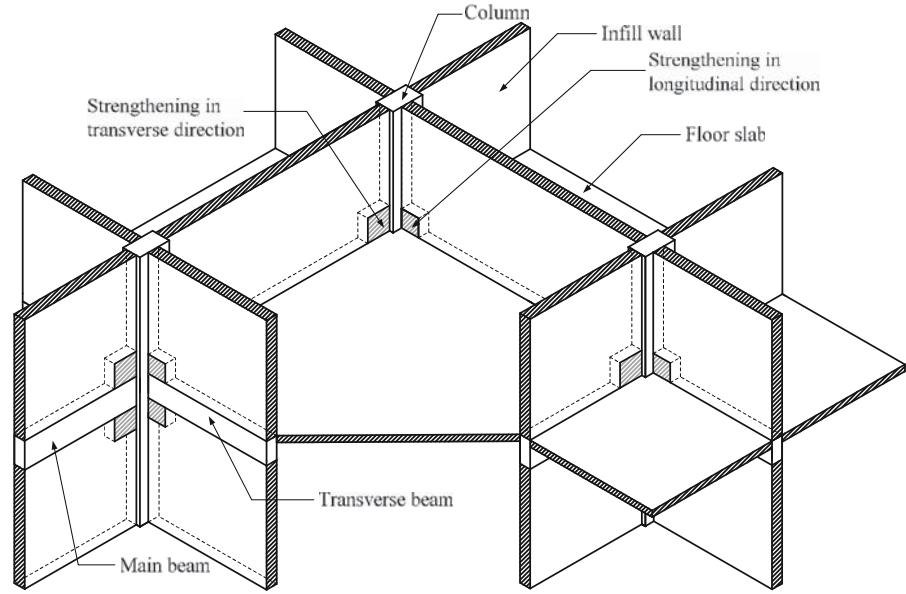
et al. [10] and Ghobarah et al. [11]. The steel jacketing has proved successful in upgrading the shear strength of the joint. However, the corrosion potential and the need to fireproof the added steel elements posed a challenge to widespread application of the procedure.

The use of fiber-reinforced polymer (FRP) materials for increasing joint shear strength has been investigated by several researchers [12–16]. FRP composites have the advantages of fast and easy application, high strength to weight ratio and corrosion resistance. Externally bonded glass or carbon composite materials (GFRP or CFRP) are attached to the faces of the joint by using epoxy resin. Significant improvements in joint strength and ductility have been achieved.

In this paper, a joint retrofitting technique called “planar joint expansion” is proposed. In this method, the beam-column joint is two-dimensionally enlarged by cast in-situ concrete. The in-situ cast joint expansion can be independently installed in transverse and longitudinal directions (Fig. 1). The method is comparatively easy in application. No slab perforation is required. Since conventional materials are used, the method is cost-effective. In terms of architectural concern, the planar joint expansion can be hidden in infill walls or non-structural walls with less than 5% coverage area. Unlike concrete jacketing, there are no protruding parts of joint expansion, hence the full floor space is available, making the method architecturally acceptable. Besides using cast in-situ concrete as planar joint expansion, it may be possible to use steel angles to perform similar functions. The authors are conducting the experimental program to investigate the use of steel angle alternative for planar joint expansion.

Like other strengthening methods, the planar joint expansion has limitations. Due to shortened member length, beams and columns are more prone to shear failure. The member stiffness also increases, which may attract more lateral seismic force. Hence, it may be necessary to examine the likelihood of member shear failure and reanalyze the structure with increased stiffness. Moreover, the method is applicable to beam-column joint that lacks sufficient joint shear capacity and beam bar anchorage bond. In case that the frame is prone to column sway mechanism, the proposed technique may not be relevant. Other suitable

**Fig. 1** 3D Beam-column frame system retrofitted with planar joint expansion



strengthening methods such as shear wall addition may be considered.

## 2 Design recommendations

The main objective of retrofit design is to avoid joint shear failure and to encourage beam flexural failure. In terms of structural performance, the planar joint expansion is designed to increase the joint shear capacity through increasing effective joint area, to improve the anchorage bond of longitudinal beam bar within the joint through increasing apparent column depth and to prevent lap splice failure of column longitudinal bars above the floor level.

As shown in Fig. 2, the horizontal joint shear force ( $V_{jh}$ ) transferred through the joint is calculated from

$$V_{jh} = T + T' - V_{cj} \quad (1)$$

where  $T$  is the tension force,  $T'$  is tension force at opposite column face and  $V_{cj}$  is column shear force.

According to the New Zealand code [17], the joint shear stress must not be greater than  $0.2f'_c$  to avoid joint shear failure. Regarding anchorage bond failure, the ACI code [18] requires the minimum column depth to bar diameter ratio ( $h_c/d_b$ ) of 20. The New Zealand standard [17] provides different equations to calculate required  $h_c/d_b$  depending on whether the frame is ductile or limitedly ductile. The requirement

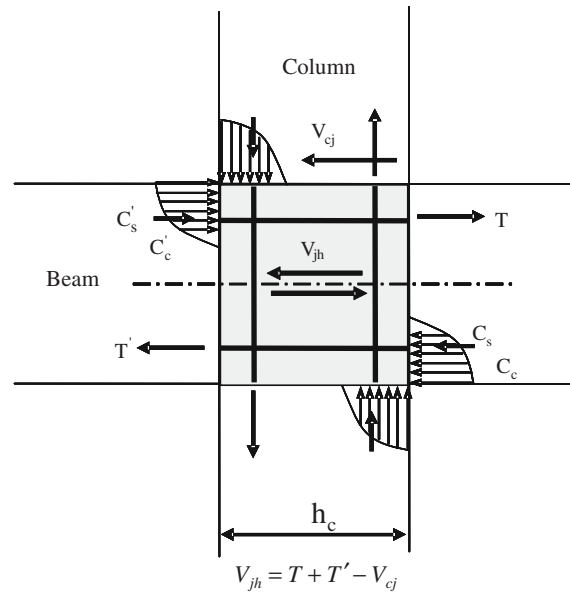


**Fig. 2** Definition of joint shear  $V_{jh}$

is given in Eqs. 2 and 3 for ductile and limitedly ductile frame, respectively.

For ductile frame

$$\frac{h_c}{d_b} \geq 1 / \left( 3.3 \alpha_f \frac{\sqrt{f'_c}}{\alpha_0 f_y} \right) \quad (2)$$

For limitedly ductile frame

$$\frac{h_c}{d_b} \geq 1 / \left( 3.9 \alpha_f \frac{\sqrt{f'_c}}{\alpha_o f_y} \right) \quad (3)$$

where  $f'_c$  is cylindrical strength of concrete;  $f_y$  is yield strength of steel;  $\alpha_f$  is 0.85 for two-way frame and 1.0 for one-way frame; and  $\alpha_o$  is 1.25 when plastic hinges in beams are developed at column faces and 1.0 when beam sections at column faces remain elastic.

The dimension of joint planar expansion is  $h_h \times h_v \times b_p$  as shown in Fig. 3. The width  $b_p$  is set equal to the beam width. Dowel bars are used to fix cast in-situ expansion to beam and column. The authors propose the following design recommendations to obtain the size and reinforcement detail of planar joint expansion,

1. The joint shear force to joint shear capacity ratio is less than 1 and joint shear stress is less than  $0.2f'_c$ . The increased effective joint shear area after retrofitting may be calculated as shown in Fig. 4.
2. The column depth to bar diameter ratio satisfies the code requirements on anchorage bond. The planar joint expansion apparently increases the column depth as shown in Fig. 4.
3. The dowel bars are designed to resist the horizontal shear arising from the difference in moment capacity of the beam section at column face and at the edge of expansion cast.

4. Beams and columns must have sufficient capacity to resist increased shear force due to shortened member lengths.
5. The retrofitting work can be carried out with ease.

### 3 Experimental program

#### 3.1 Control specimen

The experimental program consisted of three interior beam-column specimens, namely, control specimen (J0), PJE1 and PJE2. Specimen J0 represented a control un-retrofitted specimen. Specimens PJE1 and PJE2 were retrofitted by planar joint expansion. All specimens were half-scale with cruciform shape consisting of beams and columns extending from joint faces to mid-length and mid-height respectively. Since the purpose of the research was to develop a retrofitting method suitable to existing buildings, the test specimens were chosen to be as close as possible to the actual ones constructed without considering seismic effect.

For this purpose, the authors studied structural designs and drawings of ten existing buildings constructed in Thailand [5, 6]. These buildings were rigid frames with 5 to 15 stories. The building occupancy type was of essential and assembly facilities, covering schools, universities, hospitals, governmental offices and apartments. The geometrical and structural indices

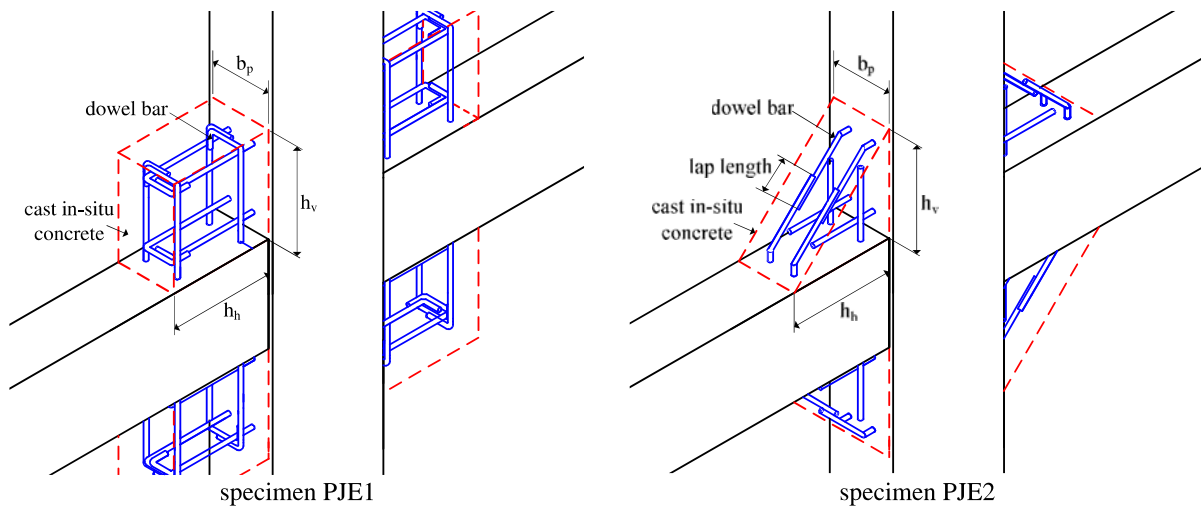
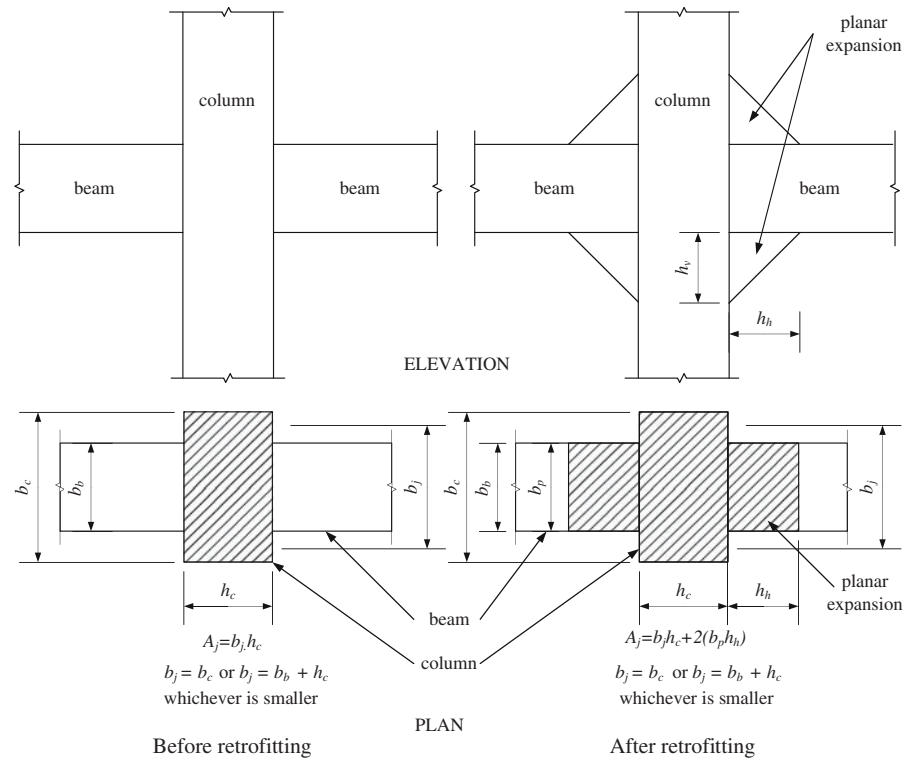


Fig. 3 3D view of planar expansion: geometry and reinforcement



**Fig. 4** Effective joint area

of substandard beam-column joint were defined for these buildings. These indices were bond index ( $BI$ ), column depth-to-beam bar diameter ratio ( $h_c/d_b$ ), beam width-to-column width ratio ( $b_b/b_c$ ), beam depth-to-column depth ratio ( $h_b/h_c$ ), column flexural capacity-to-beam flexural capacity ratio ( $M_{nc}/M_{nb}$ ), joint shear-to-joint shear capacity ratio ( $V_{jh}/V_n$ ) and volumetric joint reinforcement ratio ( $\rho_s$ ). The maximum, minimum, average and standard deviation of these indices are given in Table 1.

The half-scale control specimen (specimen J0) was designed and constructed to have geometrical and structural indices, reinforcement detail and construction method that were close to the average of the ten investigated buildings (see Table 1). The authors took the control specimen as a prototype and strengthened it by rectangular joint expansion (specimen PJE1) and triangular joint expansion (specimen PJE2).

Figure 5 shows size and reinforcement detail of the control specimen. Dimensions of column and beam sections were  $200 \times 350$  mm and  $175 \times 300$  mm, respectively. A comparison between the prototype specimen and the ACI Intermediate Moment Resisting

**Table 1** Structural indices for beam-column joint

Parameter	$BI$	$\frac{h_c}{d_b}$	$\frac{b_b}{b_c}$	$\frac{h_b}{h_c}$	$\frac{M_{nc}}{M_{nb}}$	$\frac{V_{jh}}{V_n}$	$\rho_s$
Statistical value							
Maximum	6.19	60	0.75	1.08	3.40	1.17	0.00
Minimum	2.24	24	0.50	0.63	1.54	0.91	0.00
Average	4.51	37	0.68	0.84	2.36	1.16	0.00
Standard deviation	1.65	16	0.12	0.23	0.78	0.11	0.00
Control specimen	5.12	29	0.88	0.86	2.19	1.35	0.00

Note:  $BI = \frac{f_s d_b}{2 h_c \sqrt{f'_c}}$  is bond index;  $h_c/d_b$  is column depth-to-bar diameter ratio;  $b_b/b_c$  is beam width-to-column width ratio;  $h_b/h_c$  is beam depth-to-column depth ratio;  $M_{nc}/M_{nb}$  is column flexural capacity-to-beam flexural capacity ratio;  $V_{jh}/V_n$  is joint shear-to-joint shear strength ratio;  $\rho_s$  is volumetric joint reinforcement ratio

Frame [18] was conducted to identify the deviation of non-ductile reinforcement details from the code. As seen in Table 2, longitudinal reinforcements satisfied the IMRF requirement, but stirrup amounts in beams and columns did not comply with IMRF requirement especially at the end of members. It is noted that the joint contained no transverse reinforcements. The lap splice location of column longitudinal bars was just above the floor level.



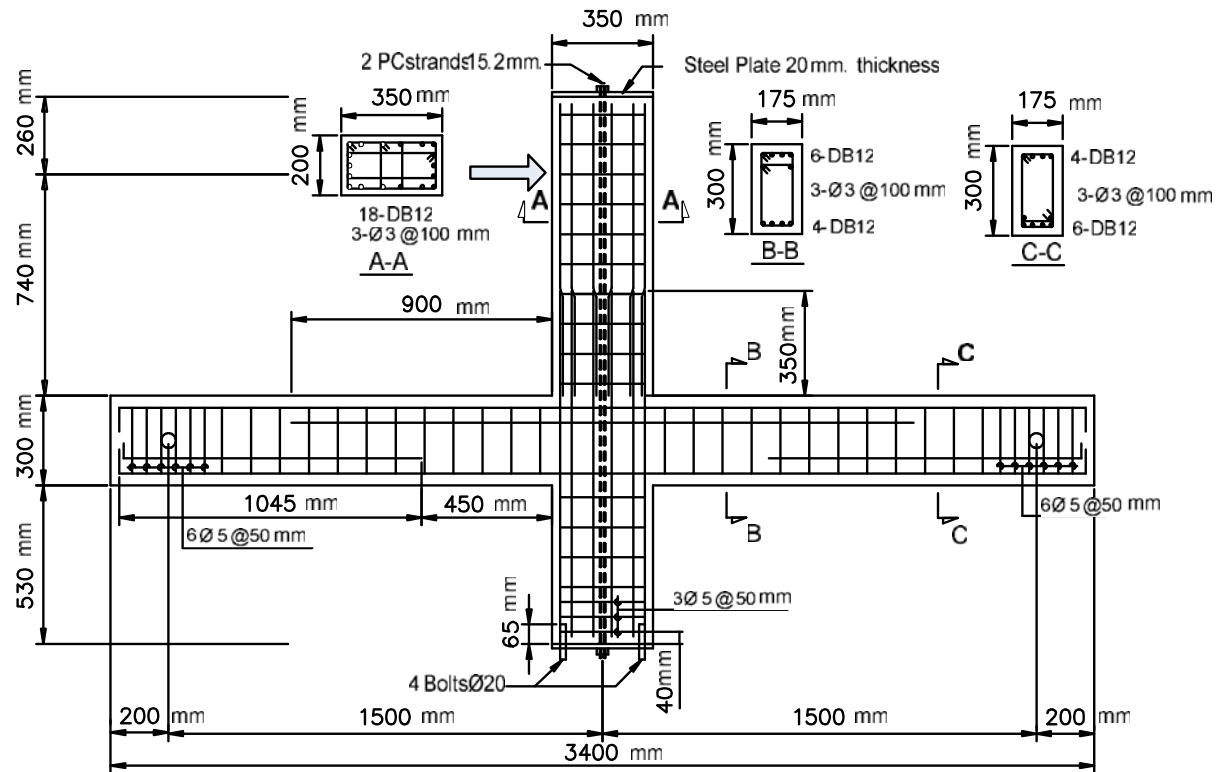


**Fig. 5** Dimension and reinforcing detail of the control specimen

**Table 2** Comparison between control specimen and ACI Intermediate Moment Resisting Frame [18]

		Specimen J0	Intermediate moment resisting frames	Compliance
Beam	Longitudinal bar	Top bar: 6-DB12	Top bar: 6-DB12	Compliant
	At column face M <sup>-</sup> , M <sup>+</sup>	Bottom bar: 4-DB12	Bottom bar: 2-DB12	
	Longitudinal bar	Bottom bar: 6-DB12	Top bar: 2-DB12	Compliant
	At any section M <sup>+</sup> , M <sup>-</sup>	Top bar: 4-DB12	Bottom bar: 2-DB12	
	Stirrup	Stirrup	Stirrup	Non compliant
	Within S <sub>0</sub>	3-RB3@100 mm	1-RB6@50 mm	
Other than S <sub>0</sub>	3-RB3@100 mm	1-RB6@120 mm		
Column	Stirrup	Stirrup	Stirrup	Non compliant
	Within L <sub>0</sub>	3-RB3@100 mm	1-RB6@90 mm	
	Other than L <sub>0</sub>	3-RB3@100 mm	1-RB6@180 mm	
	Splice	Just above floor level	No requirement	
	Location			
Joint	Within joint core	No transverse reinforcement	1-RB6@150 mm	Non compliant

Note:  $M^-$  is negative moment,  $M^+$  is positive moment,  $S_0$  is plastic hinge region of beam,  $L_0$  is plastic hinge region of column, DB12 is 12 mm diameter deformed bars, RB3 is 3 mm diameter round bars and RB6 is 6 mm diameter round bars

Main reinforcements for beam and column were 12 mm diameter deformed bars. Stirrups in beam and column ties were 3-mm diameter plain mild steel.

Table 3 shows the average tested yield and tensile strengths of these bars. The average tested cylindrical compressive strength of concrete is shown in Table 4.



**Table 3** Properties of reinforcing bar

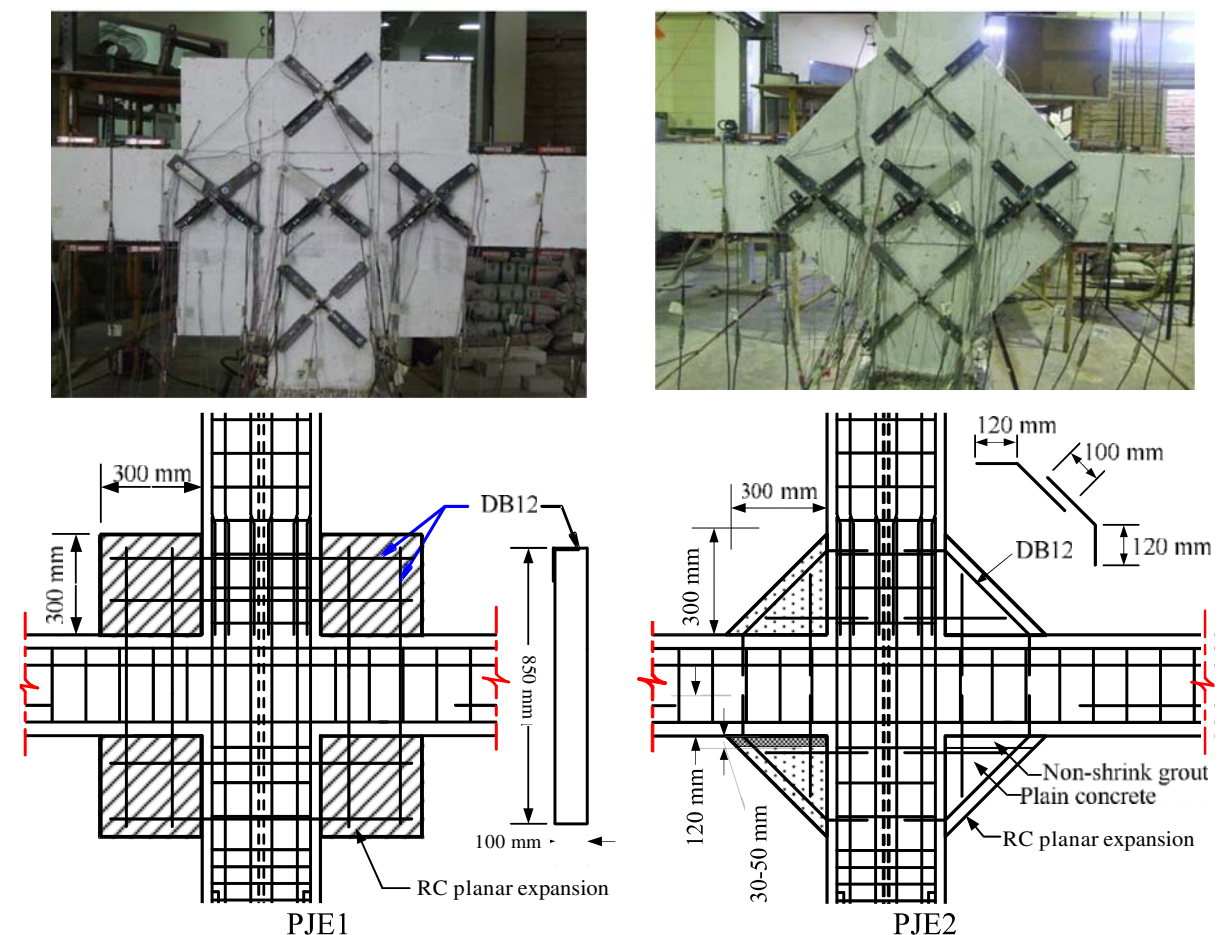
Type of reinforcing bar	Yield strength (MPa)	Ultimate strength (MPa)
DB12 SD40	480	614
wire $\phi$ -3 mm	299	373

**Table 4** Properties of concrete

Compressive strength $f'_c$ (MPa)	Control specimen (JO)	Specimen PJE1	Specimen PJE2
Top column	24.2	29.3	28.7
Beam/joint	27.3	28.3	28.7
Bottom column	23.7	28.5	30.7

### 3.2 Retrofitted specimens

The specimen size and reinforcement detail of retrofitted specimens were identical with those of the control specimen except in the retrofitted parts. The detail of planar joint expansions for specimens PJE1 and PJE2 was designed following design recommendations in Sect. 2. The joint details of retrofitted specimens, PJE1 and PJE2 were shown in Fig. 6. Considering the constructability of retrofitting work, the size of planar expansion was determined to be 300 mm in column and beam directions. Cast in-situ RC joint planar expansion with  $300 \times 300$  mm square and triangular shape was fabricated around four corners of specimens PJE1 and PJE2, respectively. The width of the expansion cast was 175 mm, the same as the beam's width.

**Fig. 6** Reinforcing detail of retrofitted specimen

Before retrofitting, the joint shear force ( $V_{jh}$ ) to joint shear capacity ( $V_n$ ) ratio is 1.35. This indicates joint shear failure. The joint shear stress in the control specimen is calculated to be  $0.26f'_c$  when steel yields and  $0.33f'_c$  when steel reaches ultimate tensile strength. The column depth to bar diameter ratio ( $h_c/d_b$ ) of the control specimen is 29. The ACI code [18] requires the minimum column depth to bar diameter ratio of 20. Based on New Zealand standard, the required  $h_c/d_b$  (Eqs. 2 and 3) is calculated to be 33 for ductile frame and 28 for frame with limited ductility. The control specimen satisfies the criterion for frame with limited ductility but does not satisfy that of ductile frame.

As a result of increased effective joint area (see Fig. 4), the horizontal joint shear stress in retrofitted specimens is reduced to  $0.1f'_c$  when steel yields and  $0.13f'_c$ , when steel reaches ultimate tensile strength. The joint shear force to joint shear capacity is also reduced from 1.35 to 0.55. The column depth to bar diameter ratio ( $h_c/d_b$ ) is increased from 29 to 79. As seen, the planar joint expansion increases  $h_c/d_b$  considerably, thus improving the anchorage bond in retrofitted specimens.

Actually, the dimension of planar expansion in the column direction ( $h_v$ ) may be smaller than 300 mm to avoid column shortening effect that may increase column shear force. However, the column of this specimen has sufficient shear capacity, thus a 300 mm dimension is selected to prevent lap splice failure of column longitudinal bars. In actual application, the trade-off among member shear failure, lap splice failure and constructability should be considered. In each piece of expansion cast, 8-DB12 (12 mm diameter deformed bars) were placed as dowels anchored in beam and column.

### 3.3 Construction method

In specimen PJE1, reinforcing steels of joint expansion cast were fabricated together with reinforcing steels in beam, column and joint. Concrete was cast together with beam and column in three lifts as shown in Fig. 7. On the other hand, for specimen PJE2, the prototype specimen was prepared first, then the joint expansion was fabricated afterwards. The construction process of specimen PJE2 is shown in Fig. 8. Dowel bars were anchored into beam and column by chemical epoxy after drilling through beam and column. The upper joint expansion was cast using concrete with the same strength as beam and column. For the lower joint expansion, however, concrete of the same strength as beam and column was poured into formworks by means of gravity flow, leaving a gap of approximately 30–50 mm beneath the bottom face of the beam to be filled with non-shrink grout (Fig. 8d). The difference in construction methods in specimens PJE1 and PJE2 was intentional, for studying any effects of construction method and construction joints formed in PJE2.

### 3.4 Test set-up, load history and instrumentation

The test set-up and boundary conditions are shown in Fig. 9. The lateral displacement was applied at the top of the column through a 500 kN hydraulic actuator. The ends of beam were supported by rollers that allowed free horizontal movement to simulate lateral drift. The bottom end of the column was supported by a hinge which allowed no movement in all directions. To simulate gravity load on column, the axial load of 12.5% column axial capacity was applied to the column by means of vertical prestressing. The column was pushed forward and pulled

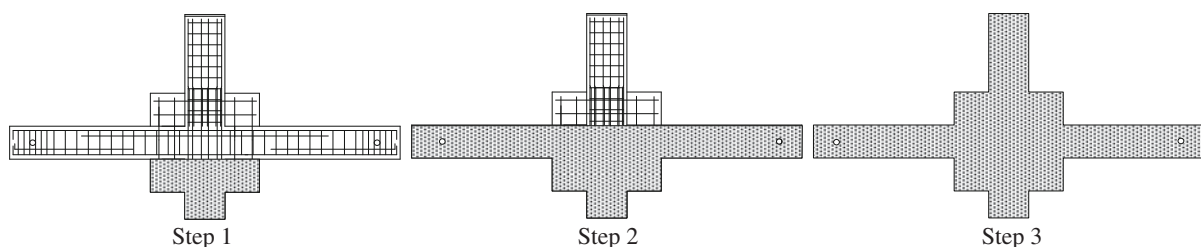
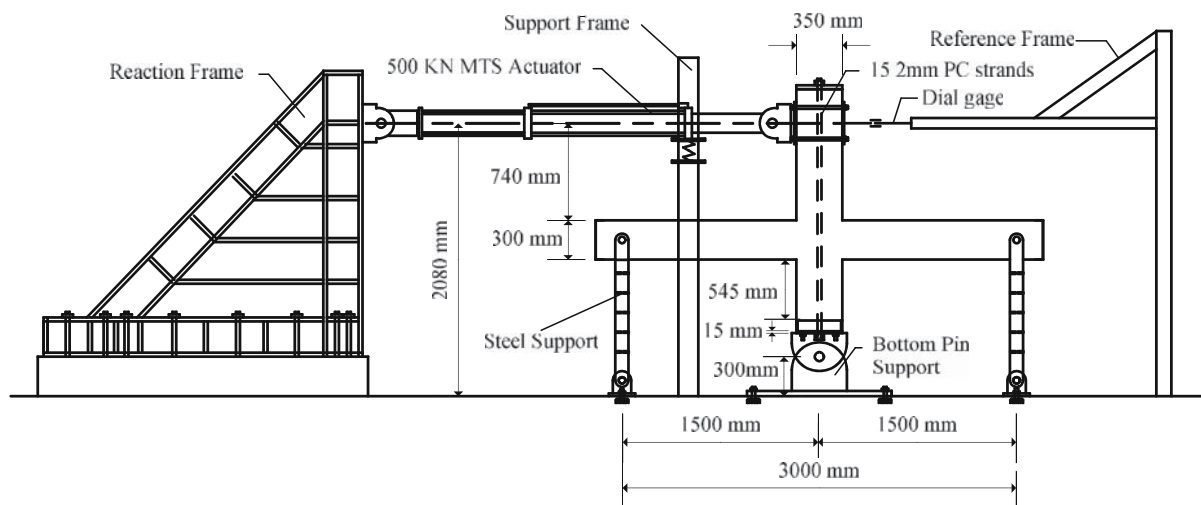


Fig. 7 Construction stages of specimen PJE1



**Fig. 8** Construction stages of specimen PJE2. (a) Drilling column and beam. (b) Inserting dowel bars and injecting epoxy into drilled hole. (c) Reinforcement after epoxy injection. (d) Casting concrete



**Fig. 9** Test set-up

backward in a reversed cyclic pattern with target drift ratios of 0.25, 0.50, 0.75%... as shown in Fig. 10. The target loop was repeated twice at each drift ratio. The load was continued until and beyond the peak load to trace the post-peak behavior. The instrumentation consisted of (1) horizontal force measurement and horizontal displacement, (2) flexural rotation in beam and column, (3) shear deformation in beam, column and joint, (4) rocking

angle at the interface between joint face and beam and (5) strains of longitudinal steels and stirrups in beam and column.

#### 4 Experimental results

The general behavior and failure character of the test specimens are studied from observed crack patterns,

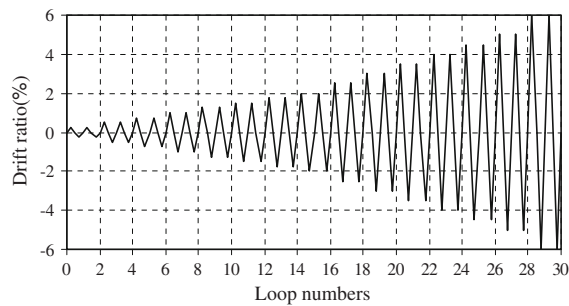


**Fig. 10** Displacement history

load-displacement hysteretic responses and strains of reinforcements. Figure 11 illustrates the observed crack patterns of each specimen during the test. Figure 12 illustrates the load-drift ratio hysteresis loops. Figure 13 exhibits strain profiles of the longitudinal bottom beam bars. The summary of test results is given in Table 5.

#### 4.1 Control specimen J0

The cracking behavior of the control specimen is illustrated in Fig. 11a. At  $\pm 0.25\%$  drift ratio, the first

flexural crack occurred in beam. At  $\pm 0.5\%$  drift ratio, the first diagonal crack occurred at joint. As drift ratio increased, these flexural and diagonal cracks grew in size and number. At  $\pm 0.75\%$  drift ratio, splitting crack occurred along longitudinal beam bar in joint. Since  $\pm 1.0\%$  drift ratio, the cracks were mainly concentrated in the joint region. These cracks formed typical X-shaped pattern as shown in Fig. 11a. The specimen reached the peak load of 72 kN at 1.75% drift ratio. At  $\pm 2.0\%$  drift ratio, the concrete in the joint spalled off, exposing column longitudinal bars. The load was continued with substantial damage in joint until  $\pm 5.0\%$  drift ratio.

As shown in Fig. 12a, the column shear force-drift ratio relation of the control specimen demonstrated elastic behavior when drift ratio was within  $\pm 0.50\%$ . Since  $\pm 0.75\%$  drift ratio, the hysteresis loops became pinched, indicating low energy dissipation upon cycling. The specimen yielded at  $\pm 1.25\%$  drift ratio and reached the peak load of 72 kN at 1.75% drift ratio. After 2.50% drift ratio, the load dropped substantially. The failure was brittle due to sudden crushing of concrete strut. After peak, the repeated cycle showed an obvious decrease in both strength

**Fig. 11** Crack observation.

- (a) Specimen J0.
- (b) Specimen PJE1.
- (c) Specimen PJE2

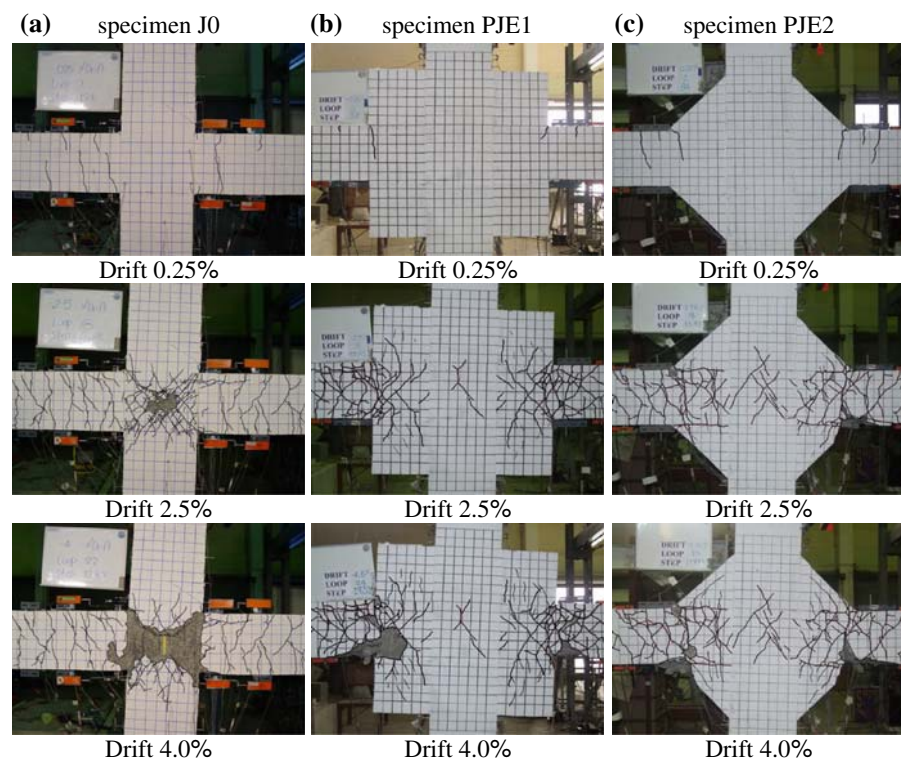
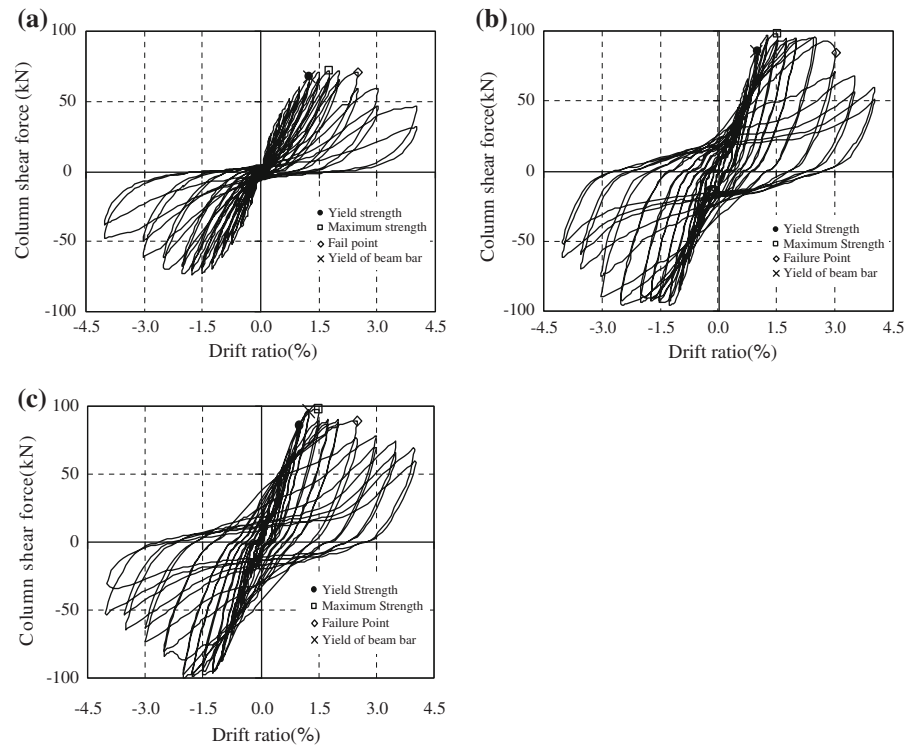




**Fig. 12** Relationship between column shear force and horizontal drift ratio.  
 (a) Control specimen J0.  
 (b) Specimen PJE1.  
 (c) Specimen PJE2



and stiffness. The ductility ratio, defined as the ratio of the maximum deformation (failure point) to elastic limit deformation (yield point) was calculated to be 2.0.

From the measured strain profiles in Fig. 13a, the largest tensile strain of longitudinal beam bar at the middle of joint was approximately 1,600 micron. The bar just reached yielding at approximately 2,400 micron strain without developing large plastic strain at column face (50 mm from the column face). Thus it can be assumed that the plastic hinge did not form in beam. As shown, the tensile strain is decreasing after 1.75% drift ratio, corresponding to the drop in peak load. However, the anchorage bond within column depth was not lost as verified from an obvious difference between strains at column face and at the middle of joint. Thus, the joint shear failure was identified as the failure mode of the control specimen.

#### 4.2 Retrofitted specimen PJE1

The cracking behavior of specimen PJE1 is illustrated in Fig. 11b. At  $\pm 0.25\%$  drift ratio, flexural crack occurred at the edge of joint expansion in beam. At

$\pm 0.50\%$  drift ratio, several flexural cracks formed in both sides of beam. At  $\pm 1.0\%$  drift ratio, diagonal cracks in beams extended and passed through the joint expansion. At  $\pm 1.50\%$  drift ratio, diagonal crack occurred in joint. Visible flexural cracks were found in beam at the edge of joint expansion on both sides at  $\pm 2.0\%$  drift ratio. At  $\pm 3.0\%$  drift ratio, concrete cover spalled off at the bottom face of beam, exposing buckled longitudinal beam bars. One leg of stirrup on both sides of the beam was broken at  $\pm 3.5\%$  drift ratio. The load was continued with significant damage in beam until  $\pm 4.0\%$  drift ratio.

The column shear force versus lateral drift ratio relation of specimen PJE1 is shown in Fig. 12b. During 0 to  $\pm 0.5\%$  drift ratio, the specimen demonstrated elastic behavior with approximately 10% higher initial stiffness than the control specimen. The yielding took place at  $\pm 1.0\%$  drift ratio when the force reached 85 kN. The specimen reached the maximum column shear force of 98 kN at 1.50% drift ratio. The maximum force was maintained until  $\pm 3.0\%$  drift ratio. The hysteresis loops of specimen PJE1 were obviously larger than that of the control specimen. The failure was flexural yielding followed by buckling of longitudinal bar and spalling of

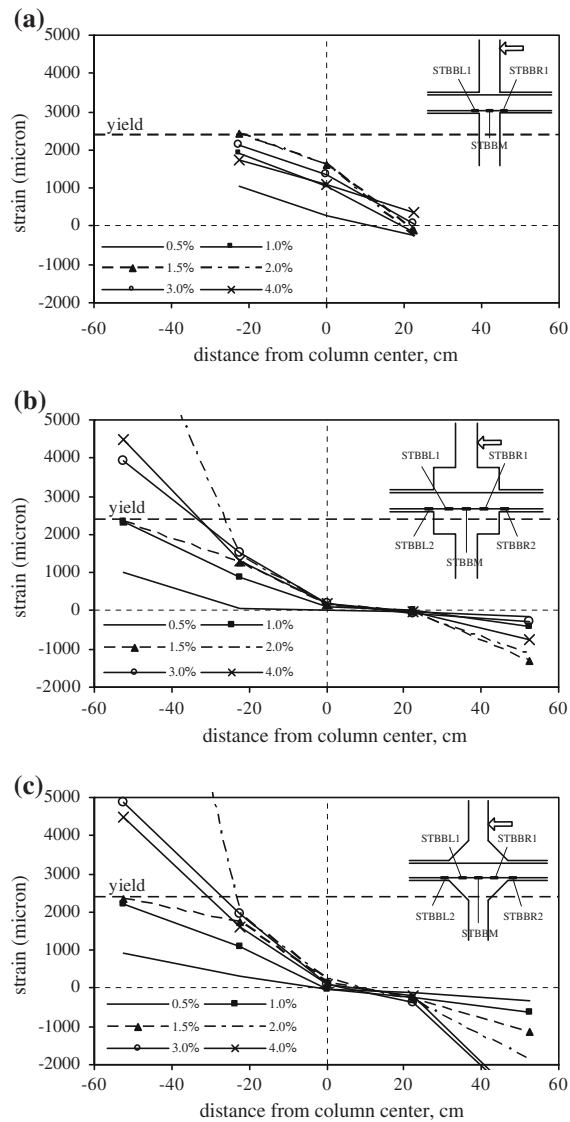


**Fig. 13** Strain along bottom beam bar. (a) Control specimen J0. (b) Specimen PJE1. (c) Specimen PJE2

concrete cover. The hysteresis loops remained stable without apparent drop in strength and stiffness until  $\pm 3.0\%$  drift ratio. The ductility ratio was calculated to be 3.0.

Measured strains along longitudinal bottom beam bar of specimen PJE1 was shown in Fig. 13b. The maximum tensile strain of longitudinal beam bar at column face (gage STBBL1) was approximately 1,500 micron, which was much less than that of the control specimen. Unlike the control specimen, however, the strain at the edge of joint expansion (gage STBBL2) reached yielding and developed large plastic strain. These strain measurements verified the effectiveness of the planar joint expansion. First, the lower strain at column face reduced the horizontal joint shear force transmitted in joint, thus preventing joint shear failure. Second, the high plastic strain developed at the edge of joint expansion indicated that plastic hinge formed in beam. Furthermore, the anchorage bond was not lost because there was an obvious difference in magnitude of strains at the middle of joint and at the edge of joint expansion.

#### 4.3 Retrofitted specimen PJE2

The cracking behavior of specimen PJE2 is illustrated in Fig. 11c. At  $\pm 0.25\%$  drift ratio, the first flexural crack occurred at the edge of joint expansion in beam. The specimen has about 18% higher initial elastic stiffness as compared with the control specimen. At  $\pm 0.75\%$  drift ratio, the horizontal crack occurred along the construction joint. Since  $\pm 1.25\%$  drift ratio, the first diagonal crack occurred in joint and stopped at  $\pm 1.75\%$  drift ratio. At  $\pm 2.5\%$  drift ratio, concrete cover at the bottom face of beam spalled off, exposing buckled bottom beam bars.

**Table 5** Summary of test result

Properties	Control specimen, J0	PJE1	PJE2
Yield strength of specimen (kN)	67.6 at 1.25% drift	85.5 at 1.0% drift	85.9 at 1.0% drift
Maximum strength (kN)	72.0 at 1.75% drift	98.3 at 1.50% drift	97.6 at 1.50% drift
Failure Point (kN)	70.2 at 2.5% drift	84.9 at 3.0% drift	89.6 at 2.5% drift
Residual strength (kN)	45.4 kN at 4.0% drift	58.2 at 4.0% drift	68.0 at 4.0% drift
Mode of failure	Joint shear failure	Beam flexural failure	Beam flexural failure
Cumulative energy dissipation at 4.0% drift ratio (kJ)	17.9	49.0	46.6
Stiffness 0–0.5% drift ratio (kN/mm)	4.57	5.02	5.41
Ductility ratio	2.0	3.0	2.5

Longitudinal beam reinforcement was fractured, leading to failure of the specimen at  $\pm 4.0\%$  drift ratio. Similar to specimen PJE1, the failure was caused by beam flexural failure.

The column shear force versus drift ratio relation of specimen PJE2 was almost the same as that of specimen PJE1 (Fig. 12). But the hysteresis loops remained stable up to only 2.5% drift ratio. The yielding took place at  $\pm 1.0\%$  drift ratio when the load reached 86 kN. The specimen reached the maximum column shear of 98 kN at 1.50% drift ratio. The yielding and maximum loads of specimen PJE2 were close to those of specimen PJE1. The ductility ratio was calculated to be 2.5.

Measured strains along longitudinal bottom beam bar of specimen PJE2 are shown in Fig. 13c. The maximum tensile strain of longitudinal beam bar at column face was the same as specimen PJE1, which was much less than that of the control specimen. The strain behaviors followed closely those of specimen PJE1. Bars developed high plastic strains at the edge of joint expansion while the strain at column face was considerably reduced. This decreased the shear stress transmitted to the joint and moved the plastic hinge to form at the edge of joint expansion rather than at the column face. The local bond pull-out was observed at the edge of joint expansion but the anchorage bond was not lost. These experimental results verified that the performance of specimen PJE2 was similar to that of PJE1.

## 5 Discussions

### 5.1 Energy dissipation

The energy dissipated by the specimen was computed as the area within hysteresis loops of the column shear force-displacement relation. The total cumulative energy dissipation (Fig. 14) was calculated as the sum of cumulative energy in the two loading directions. The comparison of energy dissipation among three specimens is illustrated in Fig. 14. The energy dissipated from the beginning till  $\pm 4.0\%$  drift ratio of control specimen J0, specimen PJE1 and PJE2 is 17.9, 49.0 and 46.6 kJ, respectively. As shown, retrofitted specimens dissipated more energy than the control specimen up to 173 and 160% for specimen PJE1 and PJE2, respectively.

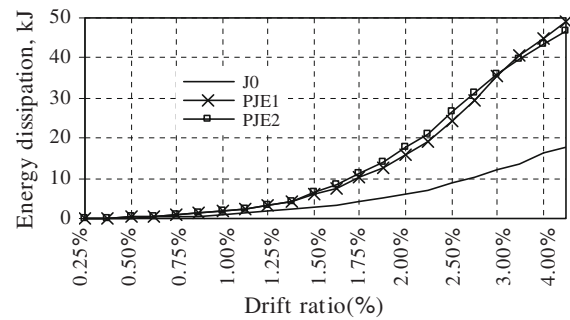


**Fig. 14** Cumulative energy dissipation

### 5.2 Joint shear deformation, beam and column flexural rotation

The joint shear deformation ( $\gamma$ ) represents the damage condition of joint. The shear deformation was measured by two displacement transducers ( $\Delta_1$  and  $\Delta_2$ ) installed diagonally with respect to the beam's axis. The average joint shear deformation was calculated from

$$\gamma = \frac{\sqrt{a^2 + b^2}}{2ab} (\Delta_1 - \Delta_2) \quad (4)$$

where  $a$  and  $b$  are horizontal and vertical distance of measuring point. The relation between joint shear deformation and drift ratio of all three specimens is presented in Fig. 15. It is apparent that the joint shear deformation of the control specimen (J0) is larger than that of retrofitted specimens. The contribution of joint shear deformation, beam and column flexural rotation to the top column displacement is shown in Fig. 16. For the control specimen, the joint shear deformation dominates the top displacement while beam flexural rotation dominates the top displacement in retrofitted specimens. This agrees with the observed failure mode of specimens.

### 5.3 Horizontal joint shear force versus drift ratio relation

Figure 17 shows the envelope of column shear force versus drift ratio for all specimens. Figure 18 shows the envelope of horizontal joint shear versus drift ratio. The horizontal joint shear force was calculated using Eq. 1, where tension forces  $T$  and  $T'$  were calculated from measured strains of steel bars at opposite column faces via Kato's cyclic stress-strain model [19].

From Figs. 17 and 18, it is seen that while the column shear envelope of control specimen is lower than that of



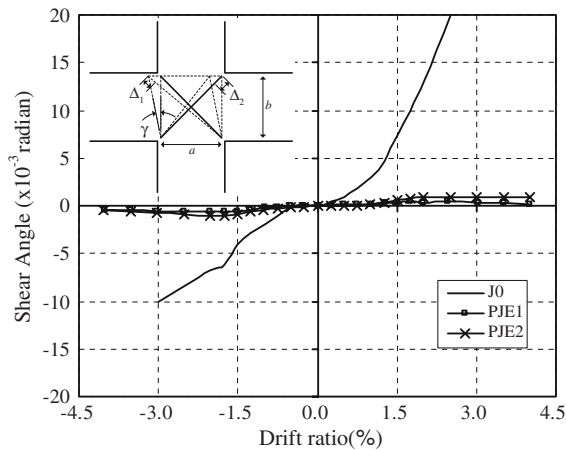


**Fig. 15** Relationship between joint shear angle and drift ratio

retrofitted specimens, the horizontal joint shear is greater. The lower horizontal shear transmitted to the joint of retrofitted specimens is due to lower tensile strains in steel bars at column faces. Thus the joint expansion reduces the joint shear stress transmitted to the joint and protects the joint from shear failure.

Figure 19 shows the plot of horizontal shear force obtained from measured strains at column faces (solid line) and at the edge of joint expansion (dotted line) for retrofitted specimens. The horizontal shear force obtained from measured strains at column faces represents shear force transferred by joint core, while that obtained from measured strains at the edge of joint expansion represents the total shear force transferred by joint core and expansion. The difference between the two graphs represents the part of horizontal shear transferred by planar expansion. Since the contribution of horizontal shear by joint

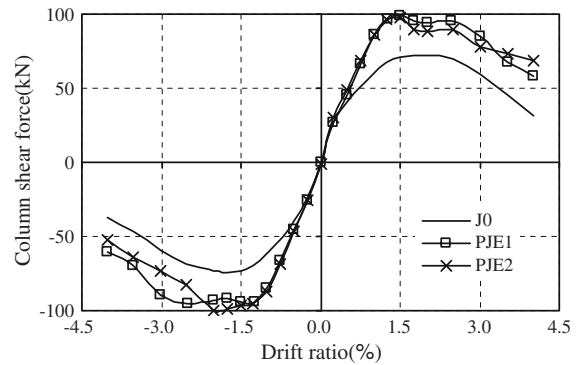


**Fig. 17** Relationship between envelope of column shear force and drift ratio

core and by expansion varies with drift ratio, the area under the graph is used to compare relative contribution. The contribution of shear resisted by joint expansion to total shear is 40 and 26% in specimens PJE1 and PJE2, respectively.

#### 5.4 Joint shear stress

The horizontal joint shear stress,  $v_{jh}$ , is calculated as the horizontal joint shear force divided by the effective area of the joint. The New Zealand standard [17] requires that  $v_{jh}$  not exceed  $0.2f'_c$  to avoid diagonal compression failure in beam-column joint. For the control specimen,  $v_{jh}$  was calculated to be  $0.26f'_c$  when steel yields and  $0.33f'_c$  when steel reaches ultimate tensile strength. By converting the measured strains of steel at column faces in retrofitted specimens to stress via Kato's cyclic stress-strain law [19], the calculated joint shear stress  $v_{jh}$  is reduced to  $0.14f'_c$  and  $0.13f'_c$  in specimens PJE1 and PJE2, respectively.

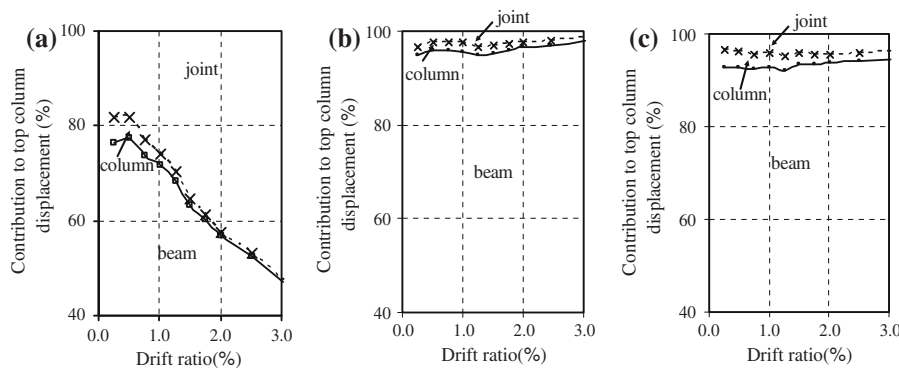


**Fig. 16** Contribution of beam, column and joint deformation to horizontal top column displacement. (a) Control specimen J0. (b) Specimen PJE1. (c) PJE2 specimen PJE2

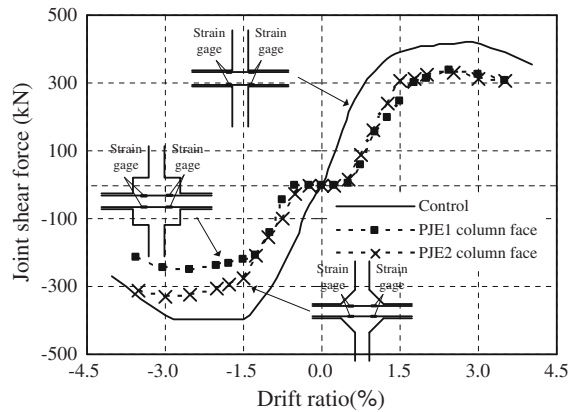


**Fig. 18** Relationship between joint shear force and drift ratio measured at column face

These values are close to pre-calculated values between  $0.1f'_c$  and  $0.13f'_c$  in Sect. 3.2. This verifies the design method of planar expansion and proves the efficiency of the proposed technique to reduce joint shear stress transmitted through joint core.

### 5.5 Comparison between specimens PJE1 and PJE2

As mentioned, the construction method of specimens PJE1 and PJE2 was intentionally different to examine the sensitivity of the proposed retrofitting method to construction procedure. The effect of construction joints formed in post-fabricated joint expansion was investigated too. Although cast in-situ afterwards, specimen PJE2 performed almost identically with specimen PJE1 in all aspects including strength,

energy dissipation, stiffness, yield and peak load and failure mode. Though horizontal cracks at the construction joint were more visible in specimen PJE2, they did not produce a significant effect on the entire behavior. The measured strains in dowels anchored into beam of specimens PJE1 and PJE2 are compared in Fig. 20. As seen, the magnitudes of dowel strain are comparable in both specimens. The dowel strain in PJE2 is slightly larger than that in PJE1. This data verifies that the construction joint does not cause an adverse effect on specimen behavior. Since dowel strains in both specimens are within elastic range, the growth of construction joint is well controlled by dowels. The post-fabricated joint expansion can be designed to produce comparable result with respect to simultaneously cast specimen.

Both retrofitted specimens failed in beam flexural failure by buckling of beam bar with moderate ductility. The performance of retrofitted specimens thus depends on the flexural behavior of beam. As mentioned, the specimen is intended to simulate existing sub-standard beam-column connection. As shown in Table 2, stirrups placed in beam and column do not comply with the requirements of ACI Intermediate Moment Resisting Frame (IMRF), hence, the retrofitted specimens show only moderate ductility. A better performance is expected if stirrups in beam and column meet the ACI requirements.

The hysteresis loops of specimens PJE1 and PJE2 were almost the same except the failure point. Specimen PJE1 failed at 3.0% drift ratio while PJE2 failed at 2.5% drift ratio. The observed prominent flexural cracks in beam were approximately located

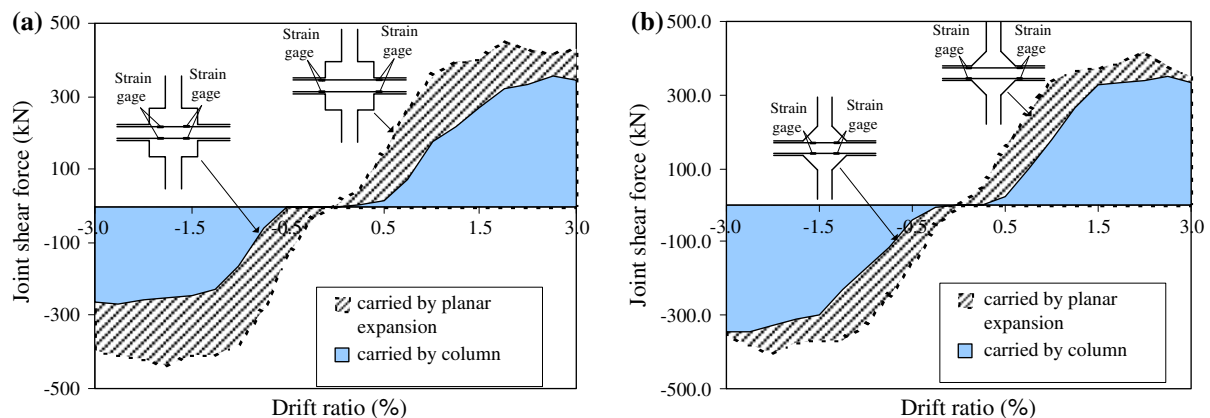
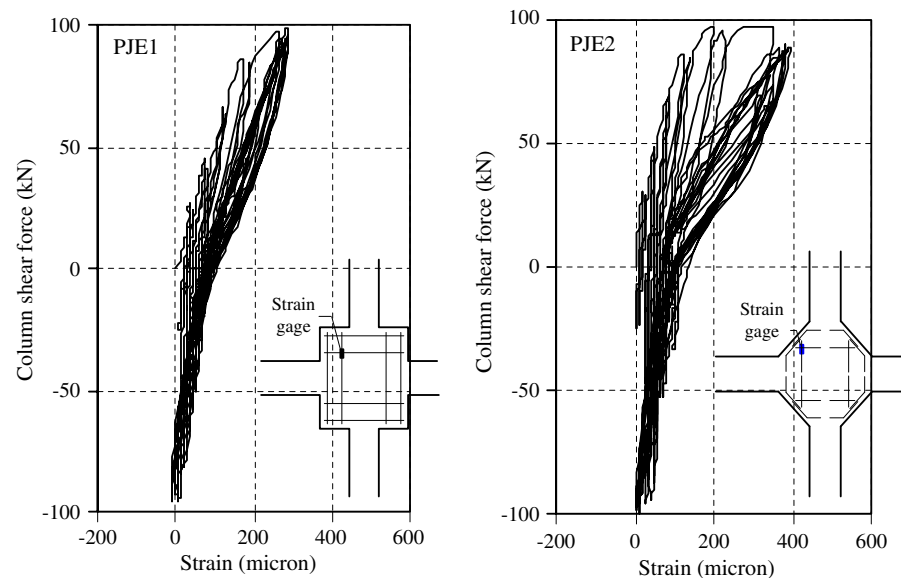


**Fig. 19** Resistance of horizontal shear force by joint core and by expansion. (a) Specimen PJE1. (b) Specimen PJE2

**Fig. 20** Relationship between column shear force and measured strains in dowels



at 300 and 250 mm from column face in specimens PJE1 and PJE2, respectively. This indicated that the plastic hinge formed at a greater distance away from column face in specimen PJE1 than in PJE2. A little inferior performance of specimen PJE2 may arise from the triangular expansion that provides lower confinement compared with square expansion in specimen PJE1. The square expansion is more effective to suppress buckling and fracture of beam bars and prevent spalling of concrete cover.

## 6 Conclusions

In this paper, a seismic retrofitting method of beam-column connection is proposed. It is based on a two-dimensional expansion of joint using cast in-situ concrete and dowel bars. An experimental program was conducted on sub-standard beam column connection to demonstrate the performance of the method. Based on the test results, the following conclusions are drawn:

1. Retrofitting substandard beam-column connection by planar joint expansion is effective to increase stiffness, ultimate strength, energy dissipation and ductility.
2. The planar joint expansion shifts the location of plastic hinge from column face to the edge of joint expansion. The failure mode is changed

from brittle joint shear failure to mixed bending and shear failure in beam.

3. A significant reduction of horizontal joint shear stress is observed in retrofitted specimens due to the reduction in strains of longitudinal beam bars at column faces. A significant increase in column depth to bar diameter ratio is also advantageous for the anchorage bond performance.
4. The triangular and rectangular joint expansion produces almost the same result. The rectangular expansion is more effective to delay spalling of concrete at compression zone in beam and buckling of longitudinal beam bars.
5. The post-fabricated joint expansion performs equally well compared with conventional construction in which the joint expansion is cast together with beam and column. Hence, the method is applicable to both new constructions and retrofitting works. The construction joints between specimens and joint expansion do not render poor cyclic behavior in retrofitted specimens.
6. Like any strengthening technique, although the joint expansion method is effective to prevent joint shear failure and to encourage plastic hinge in beam, it has limitations. The method may produce undesirable shear failure in beam and column due to shortened member length. Thus consideration must be exercised in strengthening design to prevent member shear failure.

**Acknowledgments** The authors are very grateful to Thailand Research Fund (TRF) for providing the research fund RMU4880022 to carry out the research, and to Asian Institute of Technology (AIT) for providing test facilities.

## References

1. Hakuto S, Park R, Tanaka H (2000) Seismic load tests on interior and exterior beam-column joints with substandard reinforcing details. *ACI Struct J* 97(1):11–25
2. Aycardi LE, Mander JB, Reinhorn AM (1994) Seismic resistance of reinforced concrete frame structures designed only for gravity loads: experimental performance of sub-assemblages. *ACI Struct J* 91(5):552–563
3. Kunnath SK, Hoffman G, Reinhorn AM, Mander JB (1995) Gravity-load-designed reinforced concrete buildings-Part I: seismic evaluation of existing construction. *ACI Struct J* 92(3):343–354
4. El-Attar AG, White RN, Gergely P (1997) Behavior of gravity load designed reinforced concrete buildings subjected to earthquakes. *ACI Struct J* 94(2):133–145
5. Warnitchai P (2004) Development of seismic design requirements for buildings in Bangkok against the effects of distant large earthquakes. Proceedings of the 13th world conference on earthquake engineering, Vancouver, Canada, 2004
6. Chaimahawan P, Pimanmas A (2006) Seismic vulnerability of existing reinforced concrete building in Bangkok. Paper presented at the 5th international symposium on new technology for urban safety of mega cities in Asia, Phuket, Thailand, November 2006
7. Park R, Paulay T (1975) Reinforced concrete structures. John Wiley, New York
8. Supaviriyakit T, Pimanmas A, Warnitchai P (2007) Cyclic response of non-seismically detailed interior RC beam-column connection with varying column tributary area. *Mag Concrete Res* 59(5):351–365
9. Alcocer SM, Jirsa JO (1993) RC frame connections rehabilitated by jacketing. *ACI Struct J* 90(3):249–261
10. Beres A, EL-Borgi S, White RN, Gergely P (1992) Experimental results of repair and retrofitting beam-column joints test in lightly reinforced concrete frame building. Technical Report NCEER-92-0025, SUNY/ Buffalo
11. Ghobarah A, Aziz TS, Biddah A (1996) Seismic rehabilitation of reinforced concrete beam-column connections. *Earthquake Spectra* 12(4):761–780
12. Gergely I, Pentelides CP, Reavely LD (2000) Shear strengthening of RCT-Joints using CFRP composites. *J Comp Constr* 4(2):56–64
13. Ghobarah A, Said A (2002) Shear strengthening of beam-column joints. *Eng Struct* 24(7):881–888
14. Clyde C, Pentelides CP (2002) Seismic evaluation and rehabilitation of R/C exterior building joints. Proceeding of the 7th U.S. national conference on earthquake engineering, 7NCEE, Earthquake Engineering Research Institute, Berkeley, Calif, 2002
15. Antonopoulos CP, Triantafillou TC (2003) Experimental investigation of FRP-strengthened RC beam-column joint tests. *J Comp Constr* 7(1):39–49
16. Prota A, Nanni A, Manfredi G, Cosenza E (2004) Selective upgrade of underdesigned reinforced concrete beam-column joints using carbon fiber reinforced polymers. *ACI Struct J* 101(5):699–707
17. NZS 3101 (1995) The design of concrete structure. Standards New Zealand, Wellington, New Zealand
18. ACI Committee 318 (2005) Building code requirements for structural reinforced concrete and commentary (ACI318-05/318R-05). American Concrete Institute, Michigan, USA
19. Kato B (1979) Mechanical properties of steel under load cycles idealizing seismic actions. AICAP-CEB symposium on structural concrete under severe seismic actions. Rome, Bulletin D' Information 131:7–27

# Nonlinear Finite Element Analysis of Non-Seismically Detailed Interior Reinforced concrete Beam-Column Connection under Reversed Cyclic Load

Teeraphot Supaviriyakit<sup>a</sup>, Amorn Pimanmas<sup>a\*</sup> and Pennung Warnitchai<sup>b</sup>

<sup>a</sup> School of Civil Engineering and Technology, Sirindhorn International Institute of Technology, Thammasat University, Thailand.

<sup>b</sup> Asian Institute of Technology, Thailand.

\* Corresponding author, E-mail: amorn@siit.tu.ac.th

Received 2 Mar 2007

Accepted 19 Oct 2007

**ABSTRACT:** This paper presents a nonlinear finite element analysis of non-seismically detailed reinforced concrete (RC) beam-column connections under reversed cyclic load. The test of half-scale nonductile reinforced concrete beam-column joints was conducted. The tested specimens represented those of the actual mid-rise reinforced concrete frame buildings designed according to the non-seismic provisions of the American Concrete building code (ACI). The test results show that the specimens representing small and medium column tributary area failed in brittle joint shear while the specimen representing large column tributary area failed by ductile flexure though no ductile reinforcement details were provided. The nonlinear finite element analysis was applied to simulate the behavior of the specimens. The finite element analysis employed the smeared crack approach for modeling beam, column and joint, and employed the discrete crack approach for modeling the interface between beam and joint face. The nonlinear constitutive models of reinforced concrete elements consisted of coupled tension-compression model to model normal force orthogonal and paralleled to the crack and shear transfer model to capture the shear sliding mechanism. The finite element model (FEM) shows good comparison with test results in terms of load-displacement relations, hysteretic loops, cracking process and the failure mode of the tested specimens. The finite element analysis clarified that the joint shear failure was caused by the collapse of principal diagonal concrete strut.

**KEYWORDS:** beam-column connection, nonlinear analysis, joint shear failure, diagonal compressive strut, reinforced concrete plate element.

## INTRODUCTION

Although many cities in South East Asia are considered as being located in low to moderate seismic zone due to a relatively long distance from active earth faults, they are not absolutely exempt from seismic hazard. Bangkok, for example, is founded on a soft basin of marine clay of several ten-meter depths. This soil characteristic has a potential to amplify the seismic wave up to 3-4 times<sup>1</sup>. The soft ground condition is quite similar to that of Mexico City, which was devastated by 1985 Mexico earthquake with almost 10,000 death toll. Recently, the 2004 Sumatra earthquake in the Andaman Sea recorded at a magnitude of 9.3 on Richter Scale, caused violent shaking of many highrises in Bangkok though the epicenter was more than 800 kilometers away. The quake has prompted a serious public concern on seismic safety of buildings. Many tall buildings, though not designed for seismic loads, usually have shear walls to resist wind forces, and consequently may not be vulnerable to the overall collapse under the earthquake<sup>2-3</sup>. On the contrary, many low-rise and mid-

rise buildings of up to 10 stories are rigid frame without shear walls. The frame structures mainly resist lateral forces through bending of beams and columns. Most of these frame structures were designed for gravity load only according to the American Concrete building code (ACI) in Thailand, and British code (BS) in Singapore and Malaysia<sup>4</sup>.

As a result of the lack of seismic consideration in structural design, the reinforcement details of these frame buildings are usually weak against earthquake loading. As shown in Fig. 1, the deficiencies of reinforcement details are characterized by (a) little or no confining reinforcement in beam-column joint, (b) lap splice of longitudinal column bars immediately above floor level, and (c) widely-spaced column ties and beam stirrups. Under lateral force, the joint has to carry a large horizontal shear force (Fig. 2(a)) in order to equilibrate moments acting on the joint in the same direction by framing beams. Concurrently, the longitudinal beam bar in the joint is also subject to a large bond stress. As a result of these forces, the joint commonly fails by either joint shear or bar pull-out failure.

Recently, the authors have conducted a survey of existing reinforced concrete (RC) buildings in Thailand<sup>3</sup>. The building database was compiled for mid-rise RC buildings having the number of stories in the region of 5 to 15. All buildings were beam-column rigid frame without shear wall. They were designed according to the non-seismic provisions of ACI building code considering only gravity load. The buildings were grouped into 3 categories based on their column tributary area as shown in Fig. 2(b). The beam-column connections in each category were studied in terms of structural designs and reinforcement details. Three half-scale beam-column specimens that represented each building category were prepared and tested in the laboratory under reversed cyclic load. Since buildings were designed in accordance with the ACI building code, the experimental findings are supposedly applicable to not only buildings in Thailand, but also buildings designed and detailed according to the ACI code in other countries.

The experiment showed a sudden shear failure in the joint region of specimen representing connection of buildings with small and medium column tributary area (9-30 m<sup>2</sup>) and a ductile flexural failure of beam sections near the joint in the specimen representing connection of building with large column tributary

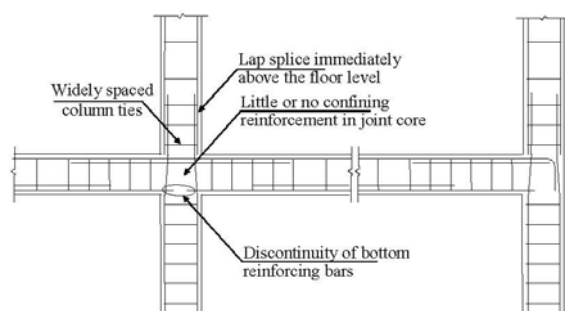


Fig 1. Typical non-seismic reinforcing detail of RC frame designed for gravity load only.

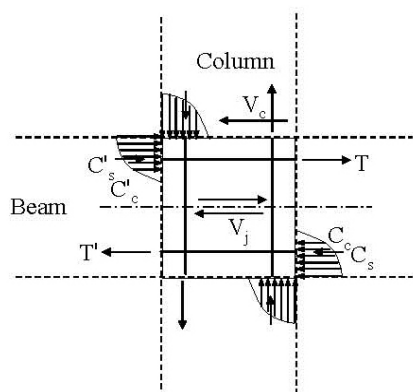
area (40-48 m<sup>2</sup>). In this paper, the authors presented the nonlinear finite element method as a tool to simulate reversed cyclic behaviors of these specimens. The beam-column joint specimens are modeled with two-dimensional plane stress elements in line with the smeared crack approach. The interface between beam and column is modeled with one-dimensional discrete joint element to simulate reinforcement pull-out. The finite element method is used to investigate the cracking process, the failure mode, the global load-displacement behavior and the principal load resistant mechanism.

## NONLINEAR FINITE ELEMENT ANALYSIS OF REINFORCED CONCRETE (RC) INTERIOR BEAM-COLUMN CONNECTION

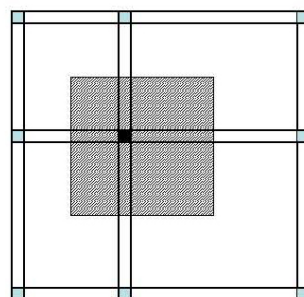
### Finite Element Model (FEM)

Fig. 3(a) illustrates a finite element model of a typical reinforced concrete (RC) interior beam-column connection of a rigid frame. The cruciform-shaped specimen is normally preferred for laboratory testing. It consists of the beam-column joint core with beams and columns extending horizontally and vertically to their mid-length where moments are assumed to be zero, i.e., point of inflection. The beam, column and beam-column regions are modeled with two-dimensional 8-node plane stress RC elements as shown in Fig. 3(b). The interfaces between beam and column are modeled with one-dimensional 6-node joint element as shown in Fig. 3(c).

The two-dimensional reinforced concrete element is constructed by combining the constitutive laws of concrete and reinforcing bar. Here, cracks and reinforcing bars are assumed to be distributed or smeared over the entire element. The bond between concrete and reinforcement is considered to be perfect, that is, concrete and reinforcement are subject to identical strains throughout the entire loading. The total stress carried by the reinforced concrete element



(a) Horizontal shear force in joint core



(b) Definition of column tributary area

Fig 2. Horizontal shear force in joint core (a) and definition of column tributary area (b).

Area (m <sup>2</sup> )	Category
9-18	Small tributary area
20-30	Medium tributary area
40-48	Large tributary area



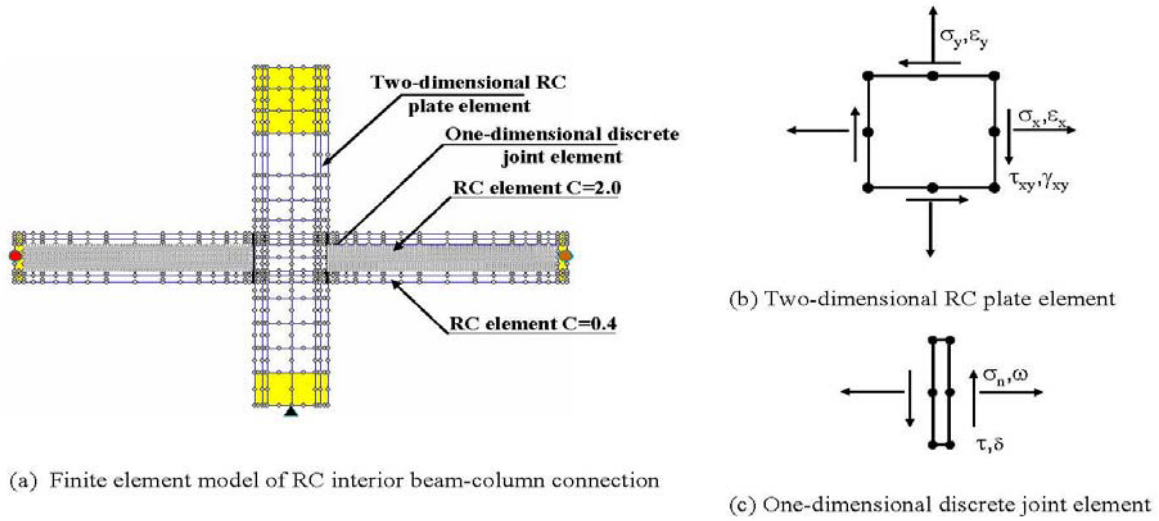


**Fig 3.** Finite element model of RC interior beam-column connection and Types of RC element.

is the sum of concrete and reinforcement stresses. In the smeared crack approach, the constitutive models of reinforcement and concrete are formulated in terms of relations between average stress and average strain as follows,

$$\{\sigma_{T,rc}\} = \{\sigma_{c,rc}\} + \{\sigma_{r,rc}\} \quad (1)$$

$$\begin{aligned} \{\sigma_{T,rc}\} &= \{\sigma_x, \sigma_y, \tau_{xy}\} \\ &= f_{rc}(\{\epsilon_x, \epsilon_y, \gamma_{xy}\}) + g_{rc}(\{\epsilon_x, \epsilon_y, \gamma_{xy}\}) \end{aligned} \quad (2)$$

where  $\{\sigma_{T,rc}\}$ ,  $\{\sigma_{c,rc}\}$ , and  $\{\sigma_{r,rc}\}$  are total stresses, concrete stresses and reinforcement stresses of RC plate element respectively;  $\{\sigma_x, \sigma_y, \tau_{xy}\}$  and  $\{\epsilon_x, \epsilon_y, \gamma_{xy}\}$  are global stress and strain respectively; and  $f_{rc}$  and  $g_{rc}$  represent constitutive laws of concrete and reinforcement, respectively. The joint element is one-dimensional with zero thickness. It represents the interface between two elements with different sectional stiffness where local discontinuities, such as reinforcement pull-out may occur. Similar to two-dimensional RC plate element, the total stresses of the joint element are the sum of concrete and reinforcement stresses. However, the constitutive laws of the joint element are formulated in terms of average stresses and relative displacements, i.e., crack opening and sliding.

$$\{\sigma_{T,j0}\} = \{\sigma_{c,j0}\} + \{\sigma_{r,j0}\} \quad (3)$$

$$\{\sigma_{T,j0}\} = \{\sigma_n, \tau\} = f_{j0}(\{\omega, \delta\}) + g_{j0}(\{\omega, \delta\}) \quad (4)$$

where  $\{\sigma_{T,j0}\}$ ,  $\{\sigma_{c,j0}\}$ , and  $\{\sigma_{r,j0}\}$  are total stresses, concrete and reinforcement stresses of RC joint element, respectively;  $\{\sigma_n, \tau\}$  is the vector of joint normal and shear stress,  $\{\omega, \delta\}$  is the vector of joint opening and sliding; and,  $f_{j0}$  and  $g_{j0}$  represent

constitutive laws of concrete and reinforcement of joint element, respectively.

Essentially, the constitutive laws for plate and joint element describe the same physical behaviors of concrete and reinforcement. However, the kinematic variables used in the constitutive formulations are different as previously explained.

The constitutive laws of concrete consist of the compressive stress model under crack closure, the tensile stress model upon crack opening and the shear stress model upon crack sliding (Fig. 4). The constitutive law of reinforcement includes the elastic-hardening model under tensile yielding, and the elasto-plastic model under compressive yielding. These laws represent major non-linearity of reinforced concrete. The combined nonlinearity of all elements subject to different stress states constitutes the entire nonlinear behavior of the specimen. In the next section, only the average stress-average strain constitutive laws of the RC plate element are presented.

### Constitutive Models of Concrete and Reinforcing Bars

#### Cracked concrete

The local strains of cracked concrete are defined with respect to the crack axis. They consist of strain normal to a crack, strain parallel to a crack and the shear strain along a crack face as shown in Fig. 4. Input variables for constitutive laws are local strains defined above as well as relevant path-dependent parameters. The constitutive laws are formulated for both envelope and hysteretic loops. Under cyclic load, two sets of diagonal cracks are generated and alternate between opening and closing in accordance with the load direction. At any load step, however, only a set of cracks is active and principally contributes to the nonlinearity of the element. The active crack is defined



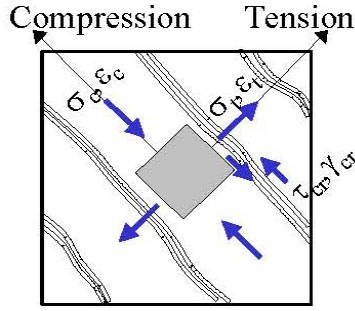


Fig 4. Local stresses and strains of cracked concrete.

as the one that has the largest normal tensile strain. The constitutive laws are expressed with respect to the active crack. In the following, the three previously mentioned constitutive laws are described.

(a) *Combined compression-tension model for normal stress orthogonal and parallel to a crack.*

The constitutive law for computing normal stress orthogonal and parallel to a crack is shown in Fig. 5. On the tensile side, the model covers both tension softening and tension stiffening behavior. After crack occurs, the tensile stress sharply drops in the un-reinforced element while it gradually decreases in the reinforced element as a result of bond between concrete and steel bar. To represent both behaviors under the same formulation, the following equation is adopted for concrete tensile stress.

$$\sigma_t = f_t \left( \frac{\varepsilon_{tu}}{\varepsilon_t} \right)^c \quad (5)$$

where  $\sigma_t$  and  $\varepsilon_t$  is the tensile stress and strain orthogonal to a crack, respectively,  $f_t$  is the concrete tensile strength,  $\varepsilon_{tu}$  is the cracking strain, and  $c$  is a softening/stiffening parameter. By varying the parameter  $c$ , the above model can cover both softening and stiffening behavior. In this paper, the parameter  $c$  is set to 2.0 and 0.4 for un-reinforced and reinforced elements to represent softening and stiffening behaviors respectively.

To compute the compressive stress parallel to a crack, the following elasto-plastic fracture model<sup>6</sup> is used

$$\sigma_c = \omega K_0 E_{c0} (\varepsilon_c - \varepsilon_p) \quad (6)$$

where  $\sigma_c$  and  $\varepsilon_c$  is the compressive stress and strain parallel to a crack, respectively,  $\omega$  is transverse tensile strain factor,  $K_0$  is the fracture parameter,  $E_{c0}$  is the initial stiffness, and  $\varepsilon_p$  is the compressive plastic strain. The fracture parameter ( $K_0$ ) and compressive strain ( $\varepsilon_p$ ) are the key parameters of the model. They are empirically formulated as<sup>6</sup>.

$$K_0 = \exp \left( -0.73 \frac{\varepsilon_c}{\varepsilon'} \left( 1 - \exp \left( -1.25 \frac{\varepsilon_c}{\varepsilon'} \right) \right) \right) \quad (7)$$

$$\varepsilon_p = 2\varepsilon' \left( \frac{\varepsilon_c}{\varepsilon'} - \frac{20}{7} \left( 1 - \exp \left( -0.35 \frac{\varepsilon_c}{\varepsilon'} \right) \right) \right) \quad (8)$$

where  $\varepsilon'$  is the concrete strain at peak compressive strength.

The model combines the nonlinearity caused by plasticity through plastic strain and fracturing damage through fracture parameter. These parameters account for the permanent deformation and irrecoverable loss of elastic strain energy, respectively. In addition, the concrete compressive strength is reduced owing to the presence of transverse tensile strain<sup>6-8</sup>. This is taken into account by an additional damage factor ( $\omega$ ) in equation 6. The lower limit of  $\omega$  depends on the compressive strength of concrete. It varies linearly from 0.4 to 0.6 as concrete compressive strength increases from 20 to 100 MPa. The relation between  $\omega$  and transverse tensile strain is shown in Fig. 5.

(b) *Shear stress transfer model*

For computing shear stress transmitted along a crack face, the contact density model<sup>6</sup> is adopted as shown in Fig. 6. The equation of the shear envelope may be expressed as,

$$\tau_{cr} = f_{st} \frac{\beta^2}{1 + \beta^2} \quad (9)$$

where  $f_{st}$  is interface shear strength along the crack and may be expressed as,

$$f_{st} = 3.8 (f'_c)^{1/3}, \text{ MPa} \quad (10)$$

$\beta$  is the normalized shear strain defined as,

$$\beta = \frac{\gamma_{cr}}{\varepsilon_t} \quad (11)$$

### Model of reinforcing bars

Local strains of reinforcing bar are defined with respect to the bar axis. For reinforcing steel, local

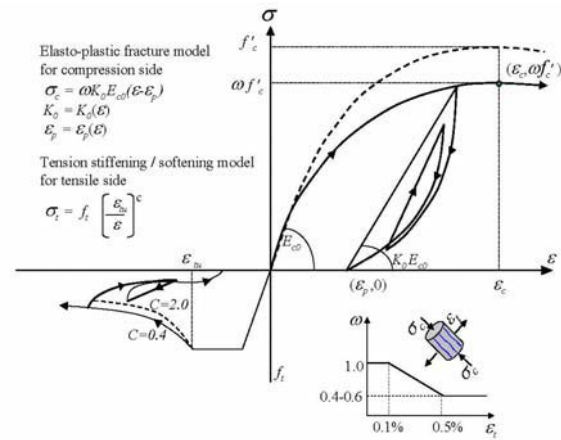


Fig 5. Combined compression-tension model for normal stress parallel and orthogonal to a crack.

yielding at the vicinity of cracks has to be taken into account in the constitutive formulation. Since reinforcement sections close to cracks are subject to yielding first whereas others are still elastic, all reinforcement sections are not simultaneously yielding throughout the entire length. This causes the apparent reduction in the average yield strength of reinforcing bars. The average yield strength of reinforcing bars embedded in concrete may be expressed as <sup>9</sup>,

$$\bar{f}_y = f_y - \frac{f_t}{2\rho} \quad (12)$$

where  $\bar{f}_y$  is an average yield strength of reinforcing bar embedded in concrete,  $f_y$  is the yield strength of bare bars,  $f_t$  is the tensile strength of concrete and  $\rho$  is the reinforcement ratio.

The model of reinforcing bar for both envelope and hysteretic loops<sup>6</sup> is shown in Fig. 7. The figure also shows that of bare bar for comparison.

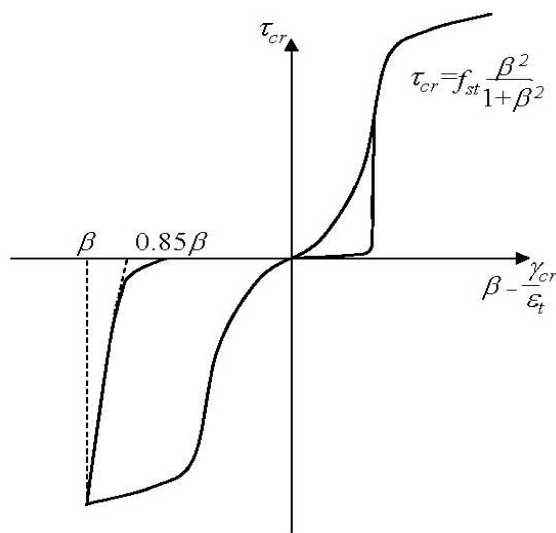


Fig 6. Shear stress transfer model.

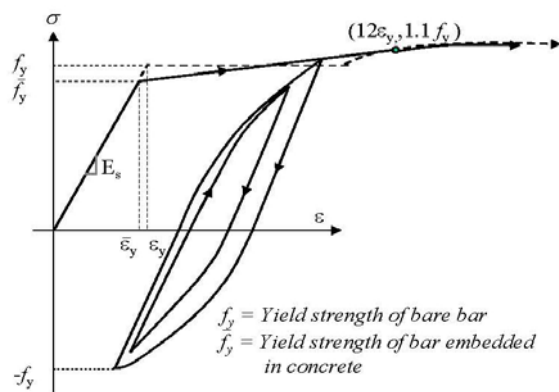


Fig 7. Modeling of reinforcing bar.

## Numerical Simulation of RC Beam-Column Connection

### Test of Non-Seismically Detailed Interior Beam-Column Connection

The authors conducted the reversed cyclic test of three half scale interior beam-column joint specimens. These specimens represented those of actual buildings designed and detailed according to the non-seismic provisions of ACI building code. The database of ten reinforced concrete mid-rise buildings in Bangkok was compiled. These buildings have 5-15 stories and were constructed as reinforced concrete frame without shear wall. The types of buildings cover university, school, apartment and hospital. The buildings were grouped into three categories based on the sizes of the column tributary area (Fig. 2(b)), as buildings with large, medium and small column tributary area. Based on the collected data, the area range is set to 40-48 m<sup>2</sup>, 20-30 m<sup>2</sup> and 9-18 m<sup>2</sup> for the large, medium and small categories, respectively. In order to characterize the structural behavior of the beam-column connection, the structural indices were defined for the beam, column and beam-column joint. The structural indices of the beam included tension and compression reinforcement ratio, shear span-to-depth ratio, flexural capacity-to-shear capacity ratio, and transverse reinforcement ratio. The structural indices of the column included axial force ratio, shear span-to-depth ratio, flexural capacity-to-shear capacity ratio, longitudinal reinforcement ratio, and transverse reinforcement ratio. The structural indices of the beam-column joint included column depth-to-bar diameter ratio, column width-to-beam width ratio, column depth-to-beam depth ratio, confinement reinforcement index, column flexural capacity-to-beam flexural capacity ratio, and joint shear-to-joint shear strength ratio.

These structural indices were calculated for each building in each category. Three half-scale beam-column specimens, namely, JL, JM and JS were constructed to represent those of each building category. The structural indices of these specimens were designed to be as close as possible to the mean values calculated from the actual building in each category. The reinforcement details and the construction methods were also as similar as possible to the actual construction. The specimen dimensions and reinforcement details are illustrated in Figs. 8 and 9. The 12-mm diameter reinforcing bar was used as longitudinal reinforcements in the beam and column. The average tested yield and tensile strengths of the bar were 499 and 615 MPa, respectively. The 3-mm diameter plain mild steel was used as transverse reinforcements in the beam and column. The tested yield and tensile strengths of the bar were 291 and 339 MPa, respectively. The average tested cylindrical compressive strength of concrete was 26.7 MPa.

The test set-up and boundary conditions are shown in Fig. 10(a). The lateral forced displacement was applied at the top of the column through a 500 kN hydraulic actuator. The ends of the beam were supported by rollers that allowed free horizontal movement to simulate lateral drift. The bottom end of the column was supported by a hinge which allowed no movement in all directions. The axial load of 12.5% of column axial capacity was applied to the column by means of vertical prestressing. The column was pushed forward and pulled backward in a reversed cyclic pattern with the target lateral drifts of 0.25%, 0.50%, 0.75%... as shown in Figs. 10(b) and 10(c). The target loop was repeated twice for each drift level. The load was continued until and beyond the peak load to trace the post-peak behavior. The experimental results shall be presented and discussed in conjunction with the numerical analysis in the next section.

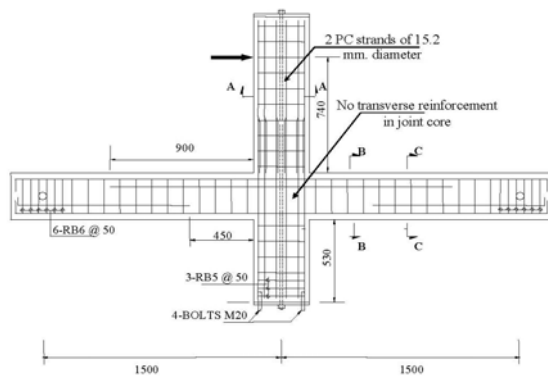


**Fig 8.** Geometry, dimension and reinforcement of all specimens (unit: mm).

### Finite Element Analysis

The typical finite element mesh of the specimen is shown in Fig. 3. For each specimen, the mesh is composed of 733 nodes, 216 two-dimensional RC plate elements and 12 one-dimensional joint elements. Loads acting on specimens include self-weight, column axial load and horizontal forced displacement. The comparison between experiment and analysis is given in Table 1. The failure is defined as the point where the applied load drops more than 80%.

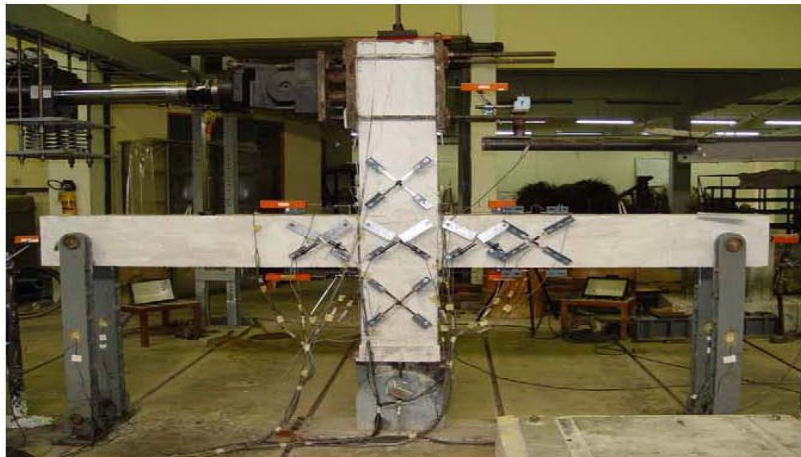
**Table 1.** Comparison between analytical (FEM) and experimental force and displacement (drift) relations.

Specimen	Force / Drift	FEM analysis	Experiment
JL	Maximum force (kN)	90	92
	Drift (%)	4.6	4.6
JM	Maximum force (kN)	73	72
	Drift (%)	2.0	1.75
JS	Maximum force (kN)	70	68
	Drift (%)	1.5	1.5

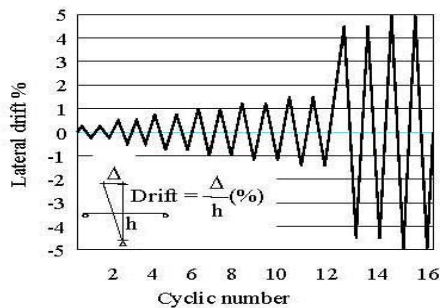
The analytical deformed shape and cracking pattern of specimen JL are compared with the experimental results in Fig. 11. The FEM demonstrates an extensive deformation at the ends of beam framing into the joints, indicating a flexural failure. The evident opening of the discrete joint element indicates pull-out of the beam reinforcing bars. The FEM also shows concentration of vertical cracks near the ends of the beams. This crack pattern indicates that bending moments act on the beam

Member	Specimen JL	Specimen JM	Specimen JS
Column section	SECTION A-A 400 300 26-DB12 STIRRUP 4-φ3 @ 100	SECTION A-A 350 200 18-DB12 STIRRUP 3-φ3 @ 100	SECTION A-A 300 200 24-DB12 STIRRUP 3-φ3 @ 100
	SECTION B-B 200 300 6-DB12 STIRRUP 3-φ3 @ 100 4-DB12	SECTION B-B 175 300 6-DB12 STIRRUP 3-φ3 @ 100 4-DB12	SECTION B-B 175 300 8-DB12 STIRRUP 3-φ3 @ 100 6-DB12
	SECTION C-C 200 300 6-DB12 STIRRUP 3-φ3 @ 100 6-DB12	SECTION C-C 175 300 6-DB12 STIRRUP 3-φ3 @ 100 6-DB12	SECTION C-C 175 300 8-DB12 STIRRUP 3-φ3 @ 100 8-DB12

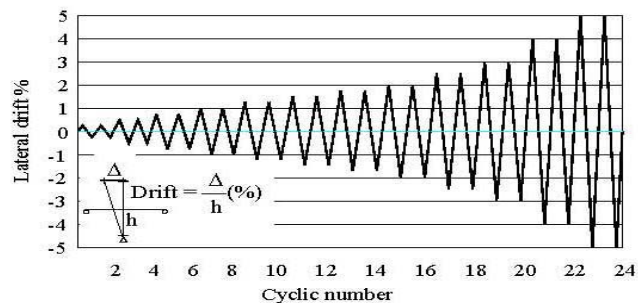
**Fig 9.** Cross section of beams and columns (unit: mm).



(a) Laboratory test set-up



(b) Displacement history of specimen JL



(c) Displacement history of specimen JM and JS

**Fig 10.** Laboratory test set-up (a) and Displacement history of each specimen (b and c).

ends in the same direction. On the contrary, the FEM predicts little distortion and cracking in the elements of the joint region. Hence the failure does not originate from the joint. Moreover, no major cracks are computed in the column adjacent to the joint core. The failure is therefore categorized as ductile strong column-weak beam. In a building with a large column tributary area, the size of the columns is usually large, whereas the span of the beams is long. This configuration leads to a large column flexural capacity, a high joint shear strength and a low beam flexural strength.

The comparison between analytical and experiment load versus applied displacement is shown in Fig. 12(a). A reasonable match is obtained for both envelope and hysteretic loops. The hysteretic loops are wide, indicating large energy dissipation. In the experiment, concrete crushing and subsequent spalling occurred in the beam and consequently exposed longitudinal and transverse reinforcements. This was followed by buckling of compression reinforcement. The spalling and reinforcement buckling are not included in the present constitutive models, hence the numerical loops are relatively wider than the experimental ones. The FEM predicts ductile yielding with long yield plateau up to 4.6% drift which is the same as the experimental

value. It shall be noticed that the sub-standard beam-column joint in buildings with large column tributary area is quite ductile though it was designed and detailed without considering seismic loads in accordance with the ACI building code. The ductility can be enhanced by providing closed stirrups near the beam's end to prevent concrete spalling and reinforcement buckling.

The analytical deformed shape and cracking pattern of specimen JM and JS are compared with experimental results in Fig. 11, respectively. In contrast to specimen JL, the mesh of JM and JS is extremely distorted, showing a large shear deformation in the joint region. The analytical cracks are mostly inclined and concentrated in the joint zone. Two sets of intersecting diagonal cracks alternate opening and closing in accordance with the change in the load direction. These cracks form the dominant X-shape pattern. The analytical joint damage and development of diagonal cracks closely follow experimental results. Some small flexural cracks are computed in the beams and columns but do not cause the failure. The failure originates from the joint zone as a result of excessive joint shear force.

The comparison between experimental and numerical load versus applied displacement relation is shown in Figs. 12(b) and 12(c) for specimen JM and JS,



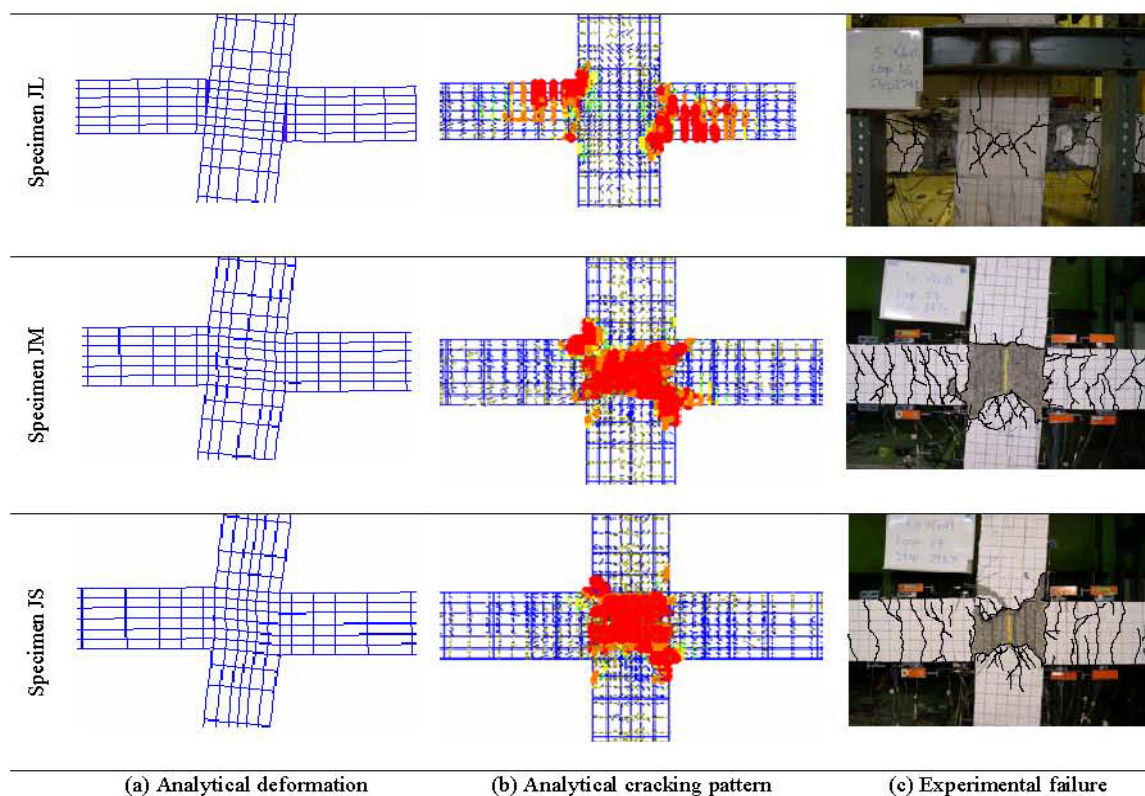


**Fig 11.** Comparison among Analytical deformation (a), Analytical cracking pattern (b), and experimental failure of each specimen (c).

respectively. The maximum experimental drifts at peak load are 1.75% and 1.5% for specimens JM and JS, respectively. The corresponding computed drifts are 2.0% and 1.5%, respectively. The hysteretic loops are narrow and pinched towards the origin, indicating small energy dissipation. This may be associated with sliding of diagonal cracks in the joint. However, the analytical loops are wider than experimental ones. This is supposedly caused by the concrete spalling in the joint area which is not included in the present analytical model. It is also observed that the attained lateral drift tends to be smaller for a substandard beam-column joint in RC frame with a smaller tributary column. This is probably because the frame is likely to have smaller column dimensions, just sufficient to carry gravity load.

The joint shear failure is undesirable because it is brittle and catastrophic. The tendency of brittleness is more evident for the beam-column connection with a smaller column tributary area. To analytically identify the failure mechanism of the joint region, the principal compressive stresses of concrete are computed from the FEM stress outputs. The development of compressive struts is compared among the three analyzed specimens in Fig. 13.

Before peak, the formation of compressive strut is dominant in all specimens. As the lateral drift increases,

the compressive stress rapidly intensifies in specimen JS. The collapse of compressive struts generally coincides with the failure point of the specimens. As for specimen JL, the compressive strut is maintained throughout the entire loading. At 4.6% drift when failure took place, the strut remains stable, indicating that the joint is sound and does not cause failure. This observation agrees with the experimental result. This analytical results show that the diagonal strut formation is the principal load resistant mechanism for the joint of specimens JM and JS and the beam flexural yielding is the main load resistant mechanism for specimen JL.

## CONCLUSION

The paper presents the non-linear finite element analysis as a tool to evaluate the reversed cyclic behavior of the sub-standard RC beam-column connections in mid-rise frame building designed and detailed according to the non-seismic provisions of ACI building code in a low to moderate seismic region. The finite element analysis includes the nonlinearity of cracked concrete in tension, compression and shear, and yielded reinforcement in line with the smeared crack approach. It is shown that the FEM can satisfactorily reproduce the load-displacement envelope as well as hysteretic

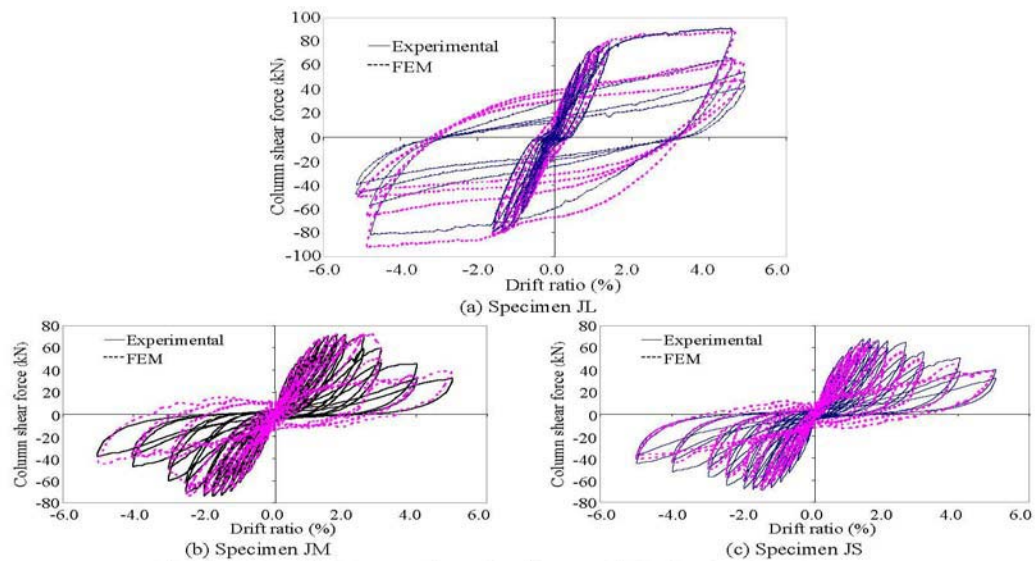


Fig 12. Relationship between column shear force and drift ratio of each specimen.

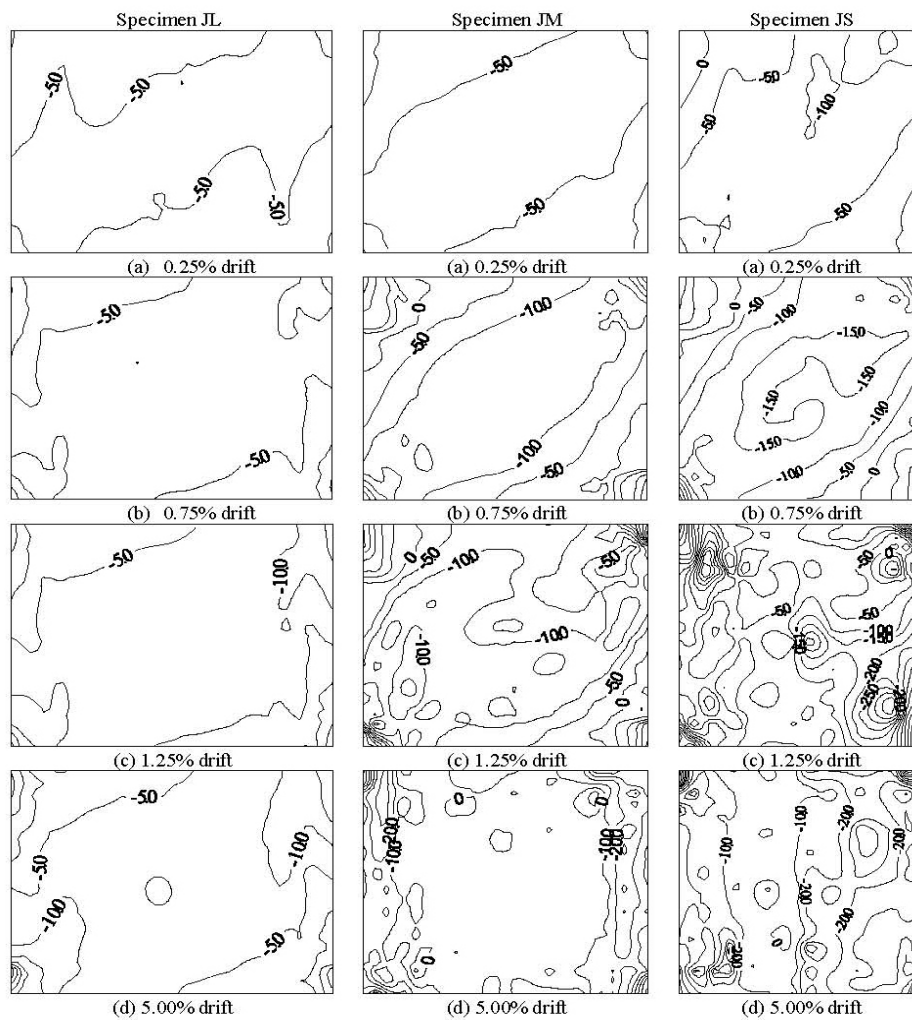


Fig 13. Principal compressive stresses (unit: MPa) of each specimen

loops of the tested specimens. As for the failure mode, the finite element analysis predicts a ductile beam flexural failure for specimen JL representing actual frame with a large column tributary area, and brittle joint shear failure for specimens JM and JS representing actual frame with a small and medium column tributary area, respectively. The collapse of compressive diagonal strut is verified to be the principal failure mechanism. The analytical failure modes, damage zones and cracking process compare well with the experimental results. However, the analytical hysteretic loops are comparatively wider than experimental ones since the nonlinearity due to concrete spalling and reinforcement buckling has not been taken into account in the present analysis.

## ACKNOWLEDGEMENTS

The authors are very grateful to Thailand Research Fund (TRF) for providing the research fund RMU4880022 to carry out the research.

## REFERENCES

1. Warnitchai P (2004) Development of seismic design requirements for buildings in Bangkok against the effects of distant large earthquakes. *Proceedings of the 13<sup>th</sup> World Conference on Earthquake Engineering, Vancouver*.
2. Aoyama H (1981) A method for the evaluation of the seismic capacity of existing RC buildings in Japan. *Bulletin of the NZ National Society for Earthquake Engineering*, 105-30.
3. Fintel M (1991) Shear walls-an answer for seismic resistance? *Construction International*, 48-53.
4. Bing L, Tso-Chien P(2004) Seismic performance of reinforced concrete frames under low intensity earthquake effects. *Proceedings of the 13<sup>th</sup> World Conference on Earthquake Engineering, Vancouver*.
5. Warnitchai P, Pimanmas A, Thinth DT(2004) Seismic performance of RC sub-assemblages with non-seismic reinforcement details. *Proceedings of the First Asian Conference for Earthquake Engineering, Phillipines*.
6. Maekawa K, Pimanmas A, Okamura H (2003) Nonlinear mechanics of reinforced concrete. Spon Press.
7. Vecchio FJ, Collins MP (1986) The modified compression field theory for reinforced concrete elements subjected to shear. *ACI Structural Journal* **83**(2), 219-31.
8. Vecchio FJ, Collins MP(1988) Predicting the response of reinforced concrete beams subjected to shear using the modified compression field theory. *ACI Structural Journal* **85**(4), 258-68.
9. Salem H, Maekawa K (2002) Spatially averaged tensile mechanics for cracked concrete and reinforcement under highly inelastic range. *JSCE J. Materials Conc. Struct. Pavements* **613**(42), 227-93.



# **Comparative Performance of a Substandard Beam-Column Joint with and Without Initial Bond Between Beam Bars and Concrete in the Joint Core**

**Teeraphot Supaviriyakit**

Graduate student, Sirindhorn International Institute of Technology,  
Thammasat University, Pathum Thani, Thailand,  
[teeraphot@hotmail.com](mailto:teeraphot@hotmail.com)

**Amorn Pimanmas**

Associate Professor, Sirindhorn International Institute of Technology,  
Thammasat University, Pathum Thani,  
Thailand, [amorn@siit.tu.ac.th](mailto:amorn@siit.tu.ac.th)

## **Abstract**

This paper presents the test of a beam-column joint with and without bond between concrete and longitudinal bar in the joint. The specimens are half-scale, typical of substandard actual beam-column joint of mid-rise reinforced concrete frame buildings constructed in Thailand. In Thailand, the design and construction of RC frames do not normally take into account the seismic loading. For the control specimen with full bonding, the failure was suddenly caused by crushing of a concrete strut. The energy was dissipated through diagonal cracks in the joint. On the contrary, for the specimen with debonded longitudinal reinforcement, little damage was observed in the joint. The joint remained sound throughout the entire loading. The deformation was concentrated as a fixed end rotation around the interface between the joint face and beam. As a result, the energy was mainly dissipated at the interface rather than at the joint. Either mode of failure was undesirable in terms of energy dissipation. However, the drop in load after peak of the debond specimen was more gradual than the abrupt crushing observed in the control specimen. The experiment shows the significance of the bond on the failure mode of reinforced concrete beam-column joints.

**Keywords :** Beam-column joint, Bond deterioration, Debond, Reversed cyclic loading, Joint shear

## **1. Introduction**

The lateral resistance of a rigid frame is derived from bending in beams and columns. Under lateral load, a beam-column joint has to transfer unbalanced moment between the beam and columns. This creates horizontal shear forces in the joint as shown in **Fig.1**. This joint shear force is found to be several times greater than shear forces in beams and columns [1, 2]. Obviously, the beam-column joint is one of the most critical components in the lateral load path of a frame. In Thailand, the design of reinforced

concrete frame buildings normally considers the gravity load only according to the ACI building code (ACI318) [3]. Hence, the member design and reinforcement detail do not meet the modern practice of seismic ductile reinforcement detailing. Particularly, the beam-column joints in these buildings lack confining stirrups and the size of a column is usually small.

The resultant forces in **Fig. 1** indicate that the joint shear force is transferred through a diagonal strut. The crushing of this strut

determines the joint shear failure. Moreover, the longitudinal beam reinforcing bar is subject to compression on one side and tension on the opposite side. This causes a significant bond force transfer between the concrete and longitudinal steel. The loss of bond changes the compressive stress in steel to tensile stress [4, 5]. As a result, the compressive force is increased to equilibrate the increased tension. Hence, it leads to a question whether the bond deterioration accelerates the crushing of the diagonal concrete strut. This paper attempts to investigate this problem by testing a beam-column joint with completely no bond between longitudinal bar and concrete in the joint. The result is compared with the control specimen where full bonding is provided. Another objective is to study the performance of substandard interior beam-column connection constructed in Thailand.

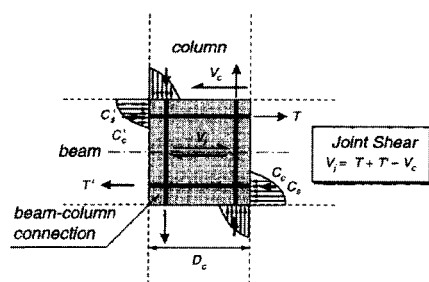


Figure 1 Joint shear force

## 2. Experimental Program

### 2.1 Specimen

The experiment was conducted to study the bond between beam longitudinal reinforcement and concrete in a substandard interior beam-column joint. The authors tested two beam-column specimens, a control and a debond specimen. The beam-column specimen was half-scale, representing the typical beam-column connection of mid-rise (6-15 storey) reinforced concrete frame buildings constructed in Thailand. The member size and reinforcement details (Fig. 2) of these two specimens were designed to closely match the average of the database of actual reinforced concrete frame building studied by Warnitchai [6] and Chaimahawan and Pimanmas [7]. The comparison of various key structural parameters of actual buildings and specimen is given in Table 1.

Note : BI = bond index =  $f_y d_b / 2h_c \sqrt{f'_c}$ ,

$h_c$  = column depth (in the direction of loading),  $h_b$  = beam depth,  $d_b$  = diameter of longitudinal bar,  $b_b$  = width of beam,  $b_c$  width of column (orthogonal to  $h_c$ ),  $M_{nc}$  = nominal moment capacity of column,  $M_{nb}$  = nominal moment capacity of beam,  $V$  = joint shear force,  $V_n$  = joint shear capacity,  $\rho_s$  = volumetric ratio of joint transverse reinforcement.

The size of beam was 175 mm x 300 mm and the size of column was 200 mm x 350 mm. The beam longitudinal reinforcements consisted of 6 DB12 (12-mm diameter deformed bar) top bars, and 4 DB12 bottom bars. The beam stirrup was 3 RB3@100 (3-mm diameter plain round bar). The column longitudinal reinforcement consisted of 18 DB12 and the stirrup was 3 RB3@100. The two specimens were identical except the bond condition of the longitudinal beam reinforcement passing through the joint core. In the debond specimen, the bond was initially removed completely by grinding the ribs of deformed bars, coating the surface with grease and wrapping the bar with plastic sheet

### 2.2 Material properties

The tested material properties are given in Tables 2 and 3 for the concrete and reinforcing bars, respectively.

### 2.3 Test set-up, instrumentation and load history

The experimental set-up is shown in Fig. 3. Both ends of the beam were supported by rollers that allowed horizontal movement to simulate lateral drift. The bottom end of the column was pinned to the base. The load was applied by a hydraulic actuator at the top of the column. The actuator was reacted against a 500 kN reaction frame fixed to a strong floor. In order to simulate the axial force on the column, prestressing tendons were provided in the column to supply an axial force of 300 kN. Figure 4 shows a photo of the specimen set-up in the laboratory. The instrumentation consisted of 1) horizontal force measurement and horizontal displacement, 2) flexural rotation in beam and column, 3) shear deformation in beam, column and joint, 4) rocking angle at the interface between joint face and beam, 5) strains of longitudinal steel and stirrup in beam and column.

**Table 1** Structural index for beam-column joint

Parameter Statistical value	BI	$\frac{h_c}{d_b}$	$\frac{b_b}{b_c}$	$\frac{h_b}{h_c}$	$\frac{M_{nc}}{M_{nb}}$	$\frac{V}{V_n}$	$\rho_s$
Maximum	6.19	60	1.00	1.08	3.40	1.524	0
Minimum	2.24	24	0.50	0.63	1.54	0.912	0
Average	4.51	37	0.80	0.84	2.36	1.254	0
Standard deviation	1.65	16	0.12	0.23	0.78	0.113	0
Specimen	5.09	29	0.88	0.86	1.68	1.382	0

**Table 2** Tested properties of concrete (MPa)

Compressive strength, $f_c'$ (MPa)	Control Specimen	Debond Specimen
Top column	23.7	26.8
Beam	26.8	21.7
Bottom column	23.2	25.0

**Table 3** Tested properties of longitudinal steel and stirrup

Properties	Longitudinal steel (12-mm dia. Deformed bar)	Stirrup (3-mm dia. Round bar)
Yield Strength (MPa)	488.6	312.0
Tensile Strength (MPa)	637.3	395.0
Modulus of elasticity (MPa)	$2.04 \times 10^5$	$2.04 \times 10^5$

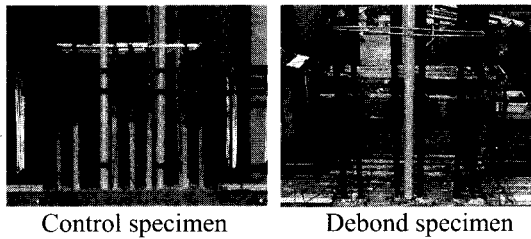
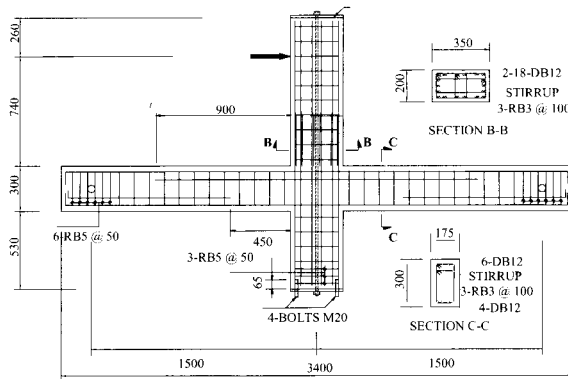


**Figure 2** Specimen dimension and reinforcement detail

The load applied to the specimen was lateral cyclic displacement-controlled. The column was pushed and pulled with increasing interstory drift of  $\pm 0.25\%$ ,  $\pm 0.5\%$ ,  $\pm 0.75\%$ ,  $\pm 1\%$  and so on as shown in Figure 5. At each drift level, the displacement was repeated twice to check the stability of the loop as well as to investigate the energy dissipation.

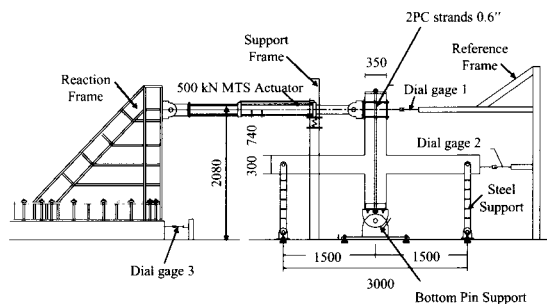


**Figure 3** Test set-up

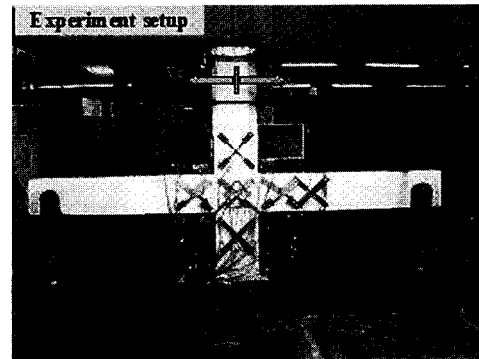


**Figure 4** Photo of specimen set-up in laboratory

### 3. Experimental results

Table 4 gives an overall summary of experimental results. First, it is seen that the control specimen had 16% greater strength than the debond specimen. The drift at peak load of the control specimen was also larger than that of the debond specimen. However, the remaining strength of the debond specimen was larger, indicating a more gentle drop in the load capacity. The failure mode was also different. The control specimen failed by joint shear failure while the debond specimen failed by beam splitting and bond pull-out failure. In the following sections, a detailed discussion shall be provided.

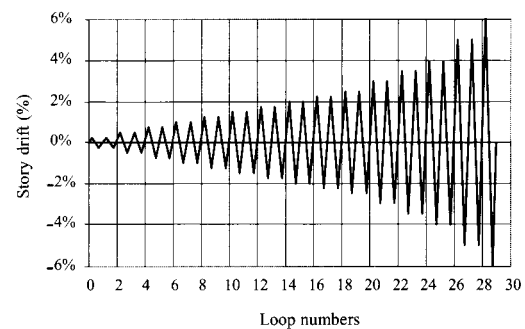


**Figure 5** Load patterns

**Table 4** Summary of test results.

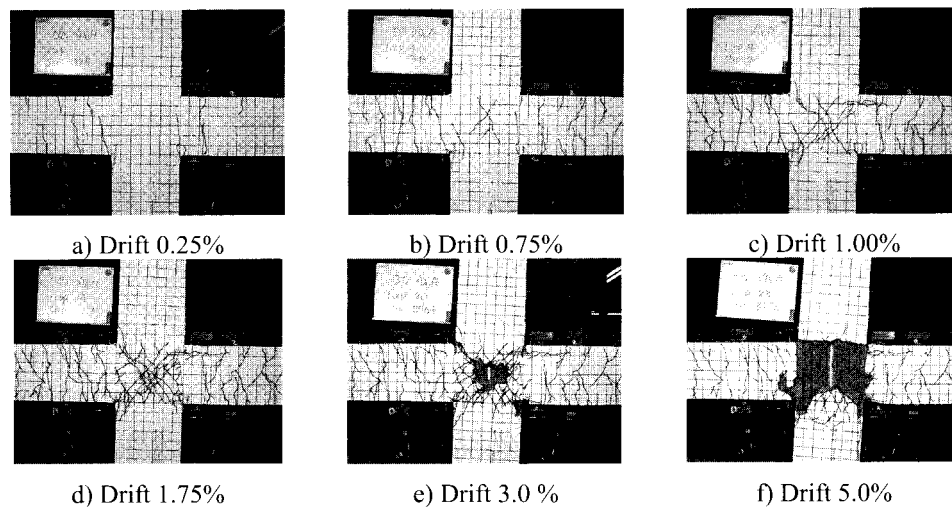
Specimen	Peak point		Residual strength at 5% drift (as percentage of peak load)	Failure mode
	Force (kN)	Drift (%)		
Control specimen	72	1.75	44	Joint shear failure
Debond specimen	62	1.50	67	Beam splitting and Bond pull-out failure

### 3.1 General observation, cracking process and failure

#### (a) Control specimen

The cracking behavior of the control specimen is illustrated in **Fig. 6**. At  $\pm 0.25\%$  drift ratio, flexural cracks developed as first cracks on the beam. At  $\pm 0.5\%$  drift ratio, the first diagonal crack occurred at the joint. As the drift ratio increased, these flexural and diagonal cracks grew in size and numbers. At  $\pm 0.75\%$  drift ratio, a splitting crack along the longitudinal beam bar in the joint was observed.

After a  $\pm 1.0\%$  drift ratio, the cracks were mainly concentrated in the joint region. These cracks were intersecting diagonal cracks with typical X-shaped pattern as shown in **Fig. 6**. On the other hand, no more flexural cracks were observed in the beam. The specimen reached a peak load of 72 kN at 1.75% drift. At  $\pm 2.0\%$  drift ratio, the concrete in the joint region spalled off, exposing column longitudinal bars. The load was continued with significant damage concentrated in the joint region until  $\pm 5.0\%$ .

**Figure 6** Crack development in control specimen

#### (b) Debond specimen

The cracking behavior of the debond specimen is illustrated in **Fig. 7**. At  $\pm 0.25\%$  drift ratio, a vertical crack was found at the interface between the joint face and beam. This crack indicated the pull-out slip of longitudinal beam bar. Flexural cracks were also observed in the beam but no diagonal crack occurred at the joint. As the drift increased, the pull-out crack widened. At  $\pm 1.0\%$  drift, the first diagonal crack

was observed in the joint. A horizontal splitting crack was also observed along the beam longitudinal bars. At  $\pm 1.25\%$  drift, the interface pull-out crack as well as the beam splitting cracks widened substantially. The beam concrete cover spalled off. In contrast, the diagonal cracks in the joint were completely inactive, leaving the joint in a sound condition until as high as  $\pm 6.0\%$  drift ratio.

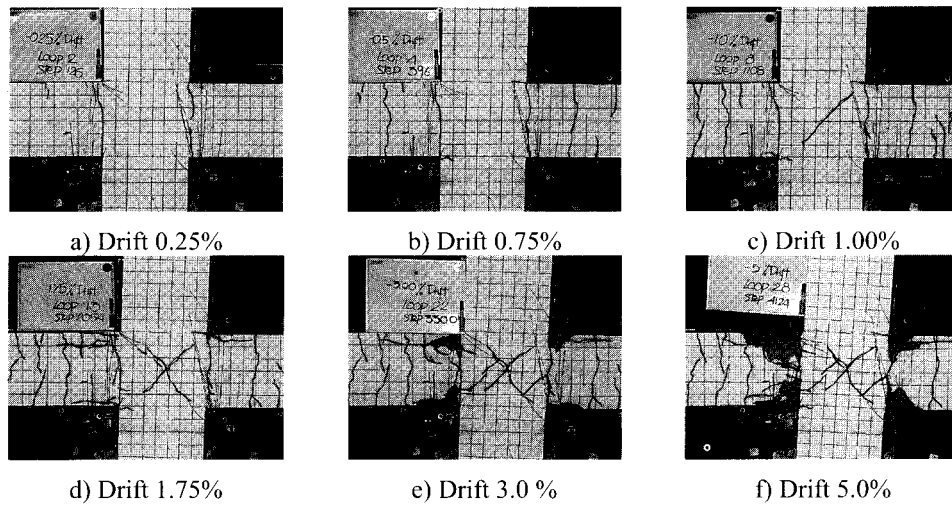


Figure 7 Crack development in debond specimen

### 3.2 Story shear versus lateral drift relation

#### (a) Control specimen

The relation between story shear and lateral drift of the control specimen is shown in **Fig. 8**. As shown in the figure, the story shear-lateral drift relation of control specimen demonstrated elastic behavior within a lateral drift of  $\pm 0.50\%$ . At  $\pm 0.75\%$  drift, the hysteresis loops became pinched, indicating low energy dissipation upon cycling. The specimen began to yield at  $\pm 1.25\%$  drift. It could resist the maximum story shear of 72 kN at 1.75% drift. Beyond 1.75% drift, the load dropped substantially. The failure behavior was brittle due to sudden crushing of the concrete strut. For any drift ratio after peak, the repeated cycle showed an obvious decrease in both strength and stiffness. The pinching in hysteresis loops became more evident, indicating a significant reduction of stiffness as a result of sliding of the diagonal crack in the joint. At 5% drift, the residual strength was 44% of the maximum load.

#### (b) Debond specimen

The story shear – lateral drift relation for the debond specimen is shown in **Fig. 9**. Elastic behavior was observed before  $\pm 0.50\%$  drift, similar to the control specimen. Moreover, the hysteresis loops were narrow and pinched as a result of an opening of a pull-out crack at the interface. The specimen reached the peak load

of 62 kN at 1.5% drift. However, the drop of peak load was not as sudden as that of the control specimen. It was supposed that the gradual reduction of peak load was caused by a gradual reduction of moment arm due to loss of the concrete compression zone on the beam's cross section. Similar to the control specimen, the repeated cycle at the drift beyond peak was unstable, and the loop was narrow with low energy dissipation. At 5% drift, the residual strength of specimen was 67% of the peak value.

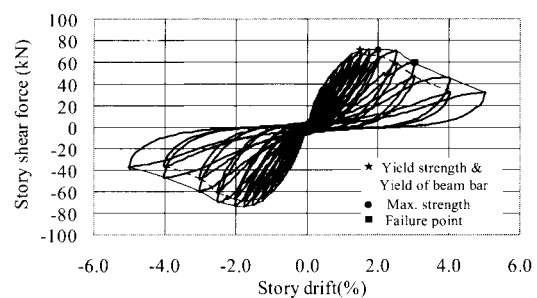
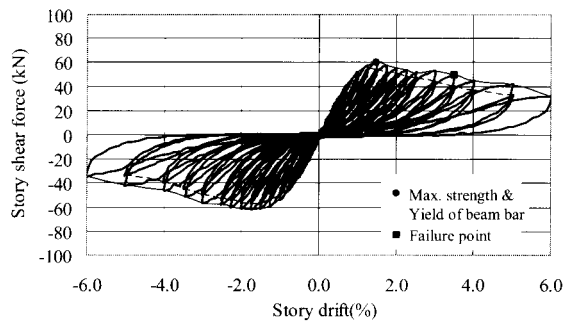


Figure 8 Story shear-story drift relation of the control specimen



**Figure 9** Story shear-story drift relation of the debond specimen

### 3.3 Joint shear deformation-story drift relation

The relation between joint shear deformation and story drift is compared between the control and debond specimen as shown in **Fig. 10**. It is seen that the joint deformation of the debond specimen is substantially lower than that of the control specimen. This is because cracks and following nonlinearity are mainly concentrated around the beam ends due to a pull-out effect. As shown in the **Fig. 11**, the column of the debond specimen was displaced laterally while the beam remained straight. This suggests that a substantial rotation must occur at the beam-joint interface due to concrete spalling and bar pull-out. The total lateral top column displacement is compatible with this interface localized rotation while the joint deformation is very small. In contrast, diagonal cracks are mainly concentrated at the joint core of the control specimen, giving rise to significant damage of concrete core resisting diagonal compression. It may be concluded that the joint shear

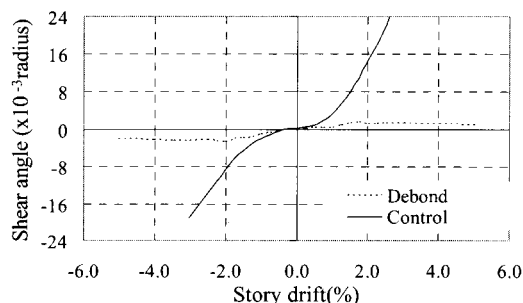


**Figure 10** Comparison of joint shear angle-story drift relation

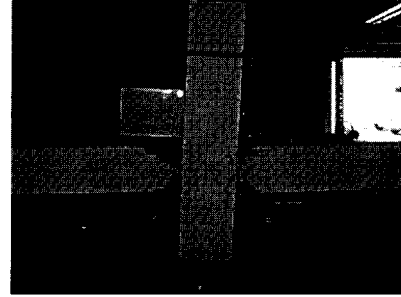


**Figure 11** Tilting of column following spalling of beam concrete

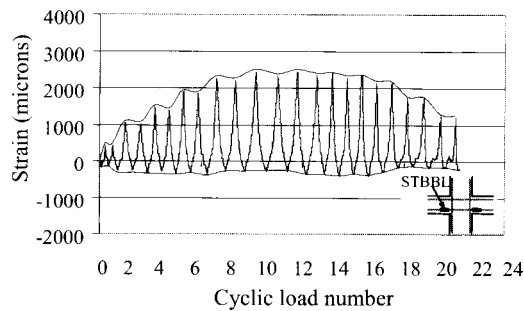
deformation causes the pinching characteristics in the control specimen while the interface localized rotation causes pinching in the debond specimen.

### 3.4 Analysis of longitudinal strains of beam bars

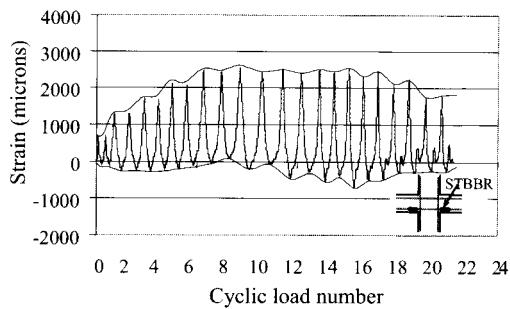
**Fig. 12** shows the strain development at each load cycle of the control specimen. The strains are measured at beam longitudinal steel at 50 mm away from the column face. For the control specimen, the steel is tensile (positive strain) on one side and compressive (negative strain) on the opposite side in early drift levels. The magnitude of compressive strain is lower since the compression force is partly carried by concrete. As the drift increases, the compressive strain is gradually changed to tensile, indicating the bond deterioration. The envelope of strain is shown in **Fig. 13**. As shown, the strain reaches a yield strain at  $\pm 1.75\%$  drift which is the peak load. After that, the strain drops. The strain drop is quite rapid even though significant bond deterioration does not yet take place. The drop in tensile strain is caused by a reduction of peak resistance due to joint crushing failure. **Fig. 14** shows the strain development at each load cycle of the debond specimen. It is seen that the specimen loses the bond from the beginning, hence, both steel sections are subject to a tension force even from the beginning of loading. Moreover, the strain in steels exceeds yield level as shown in the strain envelope in **Fig. 15**. This indicates the bars in the debond specimen maintain full yielding after peak resistance despite the nonexistence of bond in the joint. Hence, it is found that the steel could find the anchorage elsewhere even when no bonding exists in the joint core. As a result of high strains



in the beam close to the column interface, a splitting crack occurs and subsequently accelerates the concrete spalling. The reduction of peak resistance is caused by the loss of a concrete section, which leads to the movement of compressive resultant towards the beam mid-height and the reduction in the moment arm. This explains the drop in lateral load capacity of the specimen.



(a) Strain of beam bar at left side



(b) Strain of beam bar at right side.

**Figure 12** Strain of beam bar at any step of the control specimen

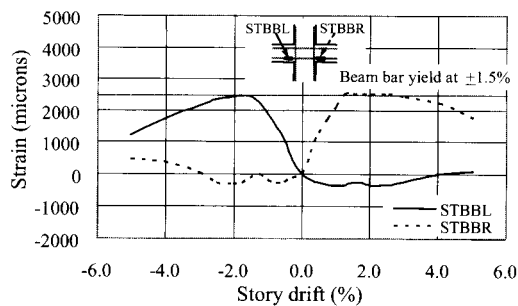
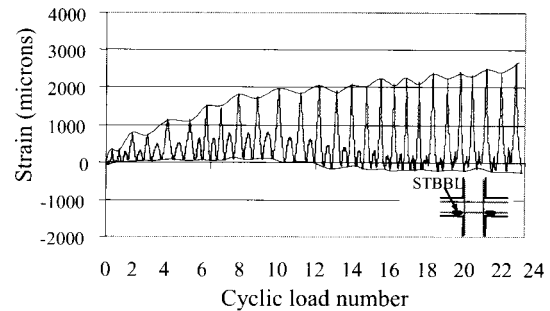
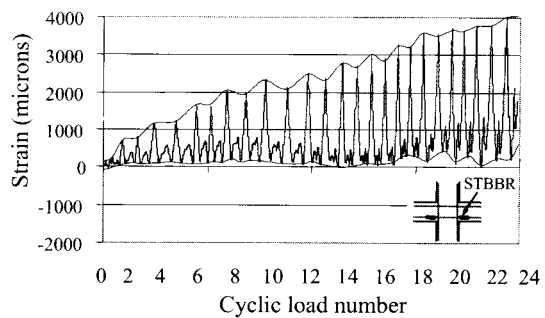


**Figure 13** Strain envelope of the control specimen



(a) Strain of beam bar at left side



(b) Strain of beam bar at right side

**Figure 14** Strain of beam bar at any step of the debond specimen

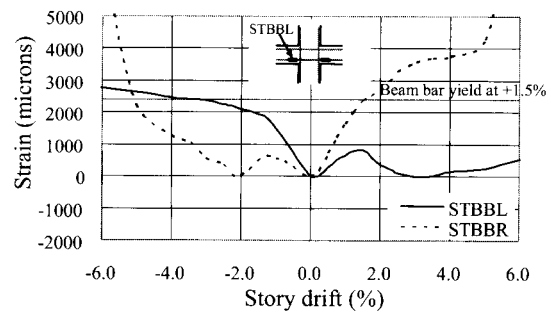


**Figure 15** Strain envelope of the debond specimen

#### 4. Failure mechanism and key structural parameters

The failure of specimens is discussed in connection with key structural parameters in this section. For the control specimen, the nominal moment capacity ratio of column to beam ( $M_{nc}/M_{nb}$ ) was 1.63, which is greater than 1.2 as required by the ACI code. Hence, plastic hinge should form in the beam according to the weak beam strong column if joint failure is not premature. However, the ratio of joint shear to nominal joint shear capacity ( $V/V_n$ ) is 1.38,

showing that the joint does not have sufficient capacity to resist shear. It should be recognized that the joint shear strength calculation is not required by ACI building codes for RC frame in low to moderate seismic zones. The ACI requires only minimum shear reinforcement to be provided in the joint core. In the control specimen, however, no stirrups are provided in the joint, causing the joint shear failure.

The bond index ( $BI = f_y d_b / 2h_c \sqrt{f'_c}$ ) and the ratio of column depth to bar diameter ( $h_c/d_b$ ) were 5.10 and 29, respectively. It is noted that no limitation of column depth to bar diameter is specified in ACI for an Intermediate Moment Resisting Frame (IMRF). For a Special moment resisting frame, the ACI sets the minimum column depth to bar diameter ratio at 20. It is found that the control specimen has not met the ACI requirement for IMRF. The specimen still showed brittle joint shear failure due to the lack of confining stirrups. In terms of bond behavior, the examination of strain of longitudinal beam bars also indicated certain bond deterioration of longitudinal bars.

As for the debond specimen, it is found that the majority of damage is concentrated in the beam close to the interface while very little damage occurs in the joint. From the strain analysis of longitudinal beam bar, it is found that steel is subject to tension on both sides of the joint in early load steps, as a result of no bond with concrete in the joint core. Hence, both top and bottom reinforcements are simultaneously subject to tension, and the concrete compressive force on the section must be doubled in order to maintain equilibrium. However, the horizontal joint shear is not correspondingly doubled. On the other hand, the horizontal shear remains almost unchanged. Figure 10 compares the horizontal joint shear under perfect bonding and debonding conditions. For perfect bonding condition, the horizontal joint shear is determined as (see Fig. 1):

$$V_j = T + T' - V_c \quad (1)$$

While for debonding condition, the equation may be written as (Fig. 16):

$$V_j = T + C' - T' - V_c \quad (2)$$

$$V_j = C' - V_c \quad \text{Since } T' = T \quad (3)$$

$$V_j = T + T' - V_c \quad \text{Since } C' = T + T' \quad (4)$$

The horizontal joint shear force should be recognized as a pseudo joint shear force as it is computed from steel forces. The actual horizontal joint shear may be less if the beam concrete cover spalls off. This mechanism is shown in Fig. 16. In this case, the horizontal joint shear is determined from concrete compressive force rather steel forces as given below.

$$V_j = C'' - V_c \quad \text{where } C'' < C' \quad (5)$$

Where  $C''$  is the resultant compressive force applied to the joint. Hence, it was seen that the actual joint shear force is less than the pseudo joint shear force for the debond specimen. Moreover, from equation (4), it is seen that although debonding doubles compressive force, it does not change the pseudo joint shear. From this analysis, it is therefore found that, the actual joint shear force is smaller than the pseudo joint shear in the debond specimen. Consequently, joint shear damage and failure do not occur in the joint.

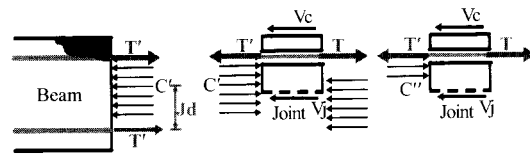


**Figure 16** Actual horizontal joint shear for the debonding case with beam concrete cover spalled off

For the debond specimen, the beam splitting crack plays a major role on the failure behavior. The beam splitting crack causes the beam concrete cover to spall off and moves the compression resultant towards the midlevel of the beam. This causes a reduction in moment capacity of the section and hence, a story shear force. The movement of compression resultant on both sides of the joint made the strut inclination flatter, and hence, more effective to resist shear. Through this mechanism, the joint of the debond specimen remains sound

throughout the entire loading. The failure is determined by the localized interface pull-out behavior.

## 5. Conclusions

The test of a beam-column joint to identify the failure mode of substandard interior beam-column connection and the effect of bond between longitudinal bars and concrete is investigated in this paper. It is found that the control specimen with full bonding fails by the crushing of a diagonal strut in the joint region. The failure is brittle. The cause of failure is due to a high value of  $V/V_n$  and the lack of joint stirrups in the joint core. In contrast, the debond specimen fails by a bond pull-out failure with significant fixed end rotation at the interface between joint face and beam. The load drop after peak is more gradual than that of the control specimen. In terms of energy dissipation, either mode of failure was undesirable as the hysteresis loops are pinched with bad energy dissipation capacity. The beam splitting crack plays a major role on the failure behavior of the debond specimen. It causes spalling of the beam concrete cover, movement of compressive resultant towards midlevel, and increases the joint shear resistance through flatter geometry of diagonal strut. The debonding of longitudinal bars in the joint core does not affect the development of strain in the steel bar. The steel can find anchorage elsewhere and develops large plastic tensile strain even after peak. The pseudo horizontal joint shear remains the same regardless of the bond condition. But the actual joint shear may be smaller under a debonding condition. As a result, the debonding reduces the

joint shear damage which is beneficial in terms of post-earthquake retrofitting.

## 6. Reference

- [1] Paulay T., and Priesley M.J.N., *Seismic Design of Reinforced Concrete and Masonry Buildings*. New York: John Wiley and Sons Inc., 1992.
- [2] Kitayama, K., Otani S. and Aoyama, H., Development of Design Criteria for RC Interior Beam-Column Joints, *ACI SP-123, Design of Beam- Column Joints for Seismic Resistance*, pp.97-123, 1991.
- [3] American Concrete Institute, *Building Code Requirements for Structural Concrete and Commentary*, Michigan, ACI committee 318, 2005.
- [4] Shiohara H., New model for Shear Failure of RC Interior Beam-column Connections, *ASCE J. Struct. Eng.*, Vol. 127, No.2, pp. 152-160, 2001.
- [5] Hakuto S., Park R., and Tanaka, H., Effect of Deterioration of Bond of Beam Bars Passing through Interior Beam-column Joints on Flexural Strength and Ductility, *ACI Struct. J.* Vol.96 No.5, pp.858-864, 1999.
- [6] Warnitchai P., Seismic Hazard Mitigation, Final Report Submitted to Thailand Research Fund (in Thai).
- [7] Chaimahawan P. and Pimanmas A., Seismic Vulnerability of Existing Buildings in Bangkok, Proceeding of the 5<sup>th</sup> Int. Symposium for Urban Safety of Mega Cities in Asia, November 2006, Phuket, Thailand (CD-ROM).



*Original Article*

## Cyclic behavior of non-seismically designed interior reinforced concrete beam-column connections

Amorn Pimanmas<sup>1</sup> and Teeraphot Supaviriyakit<sup>2\*</sup>

<sup>1</sup>*School of Civil Engineering and Technology,  
Sirindhorn International Institute of Technology, Thammasat University, Khlong Luang, Pathum Thani, 12121 Thailand.*

<sup>2</sup>*School of Civil Engineering,  
Naresuan University, Phayao Campus, Mueang, Phayao, Thailand*

Received 7 March 2007; Accepted 23 April 2008

---

### Abstract

This paper presents a test of non-seismically detailed reinforced concrete beam-column connections under reversed cyclic load. The tested specimens represented those of the actual mid-rise reinforced concrete frame buildings, designed according to the non-seismic provisions of the ACI building code. The evaluation of 10 existing reinforced concrete frames was conducted to identify key structural and geometrical indices. It was found that there existed correlation VS structural and geometrical characteristics and the column tributary area. Hence, the column tributary area was chosen as a parameter for classifying the specimens. The test results showed that specimens representing small and medium column tributary area failed by brittle joint shear, while specimen representing large column tributary area failed by ductile flexure, even though no ductile seismic details were provided.

**Key words:** substandard beam-column joint, reversed cyclic load, joint shear failure, bond deterioration, column tributary area

---

### 1. Introduction

The seismic vulnerability of old existing reinforced concrete buildings constructed in zones of low to medium seismicity was recently discussed by several researchers in the USA and New Zealand (Aycardi *et al.*, 1994, Bracci *et al.*, 1995, El-attar *et al.*, 1997, Hakuto *et al.*, 2000). Even in the South East Asian region such as Thailand, Singapore and Malaysia, which was usually believed to be safe against seismic hazard, the research in this issue has gained more attention (Li *et al.*, 2002, Li and Pan, 2004, Warnichai, 2004) due to several recent earthquake occurrences in the region. Most recently the 2004 Sumatra Earthquake in the Andaman Sea, recorded at 9.3 moment magnitude, caused violent

shaking of many buildings in Bangkok, though the epicenter was more than 800 kilometers away. The quake has prompted a serious public concern on seismic safety of buildings. In the Southeast Asian countries, there are many low-rise and mid-rise buildings of up to 10 stories constructed as beam-column rigid frames without shear walls. The frame structures mainly resist lateral forces through bending of beams and columns. Most of these structures were designed for gravity load only according to the American Concrete Institute's (ACI) building code in Thailand and British Standard (BC) code in Singapore and Malaysia.

As a result of the lack of seismic consideration in structural design, the reinforcement details of these frame buildings were usually weak against earthquake loading. The beam-column joint is one of the most critical components in the seismic load path. Under lateral force, the joint has to carry a large horizontal shear force (Figure 1) in order to

---

\*Corresponding author.  
Email address: [teeraphot@hotmail.com](mailto:teeraphot@hotmail.com)

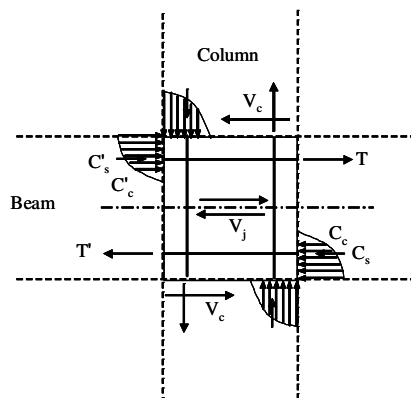


Figure 1. Horizontal shear force in joint core.

equilibrate moments acted by framing beams. Concurrently, the longitudinal beam bar in the joint is also subject to a large bond stress. As a result, the joint commonly fails by either joint shear or bar pull-out failure.

Among the experimental results of beam-column joints reported so far, the experimental works of non-seismically detailed reinforced concrete beam-column joints were still limited (Hegger *et al.*, 2003, Li and Pan, 2002, Park, 2002, Supaviriyakit *et al.*, 2006). Research in this area is still needed to form a database for building retrofitting and strengthening. In contrast to other experimental works, in which researchers presumed parameters influencing joint behavior, such as reinforcement ratio, material strength, confining hoops, column size, etc., in their experiments, this research puts more emphasis on actual existing structures. By collecting structural data and reinforcing details of existing reinforced concrete buildings, the authors defined structural and geometrical indices. Based on these indices, specimens were grouped according to the column tributary area and constructed to represent the buildings in each category.

## 2. Geometrical and structural indices of existing buildings

The authors conducted the reversed cyclic test of three

half-scale non-ductile interior beam-column joint specimens. In the past, the parameters chosen by researchers were reinforcement ratios, amount of joint confinement reinforcements, material strengths, member sizes, etc (CEB, 1996). In this research, however, instead of presuming parameters affecting beam-column joint behavior, the authors attempted to design the specimens that could represent the actual existing buildings as close to possible. First, we collected and investigated ten existing buildings to obtain the key practical structural parameters that characterized these buildings. The specimens were constructed to have the indices close to the actual ones. The specimen fabrication and reinforcing details were also made as close as the actual construction as possible. The governing parameter chosen in this study was the column tributary area. According to the investigated data, there were certain correlations between structural and geometrical indices and column tributary area, hence, it was appropriate to select column tributary area as a studied parameter.

A database of ten reinforced concrete mid-rise buildings in Bangkok was gathered. All buildings were reinforced concrete beam-column frame without shear wall and had 5-15 stories. The types of buildings covered essential facilities, including universities, schools, apartments and hospitals as shown in Table 1. These buildings were designed according to the non-seismic provisions of the ACI building code (2005) considering only gravity load. Since buildings were designed in accordance with the ACI code, the experimental findings are probably applicable not only to buildings in Thailand, but also to buildings designed and detailed according to the ACI code in general.

The buildings were grouped into three categories based on column tributary area (Figure 2(a)), as buildings with large, medium, and small column tributary area. Based on the collected data, the area range was set to 40-48 m<sup>2</sup>, 20-30 m<sup>2</sup>, and 9-18 m<sup>2</sup> for the large, medium, and small category, respectively. In order to characterize the structural behavior of beam-column connections, the structural and geometrical indices were defined for beam, column, and beam-column joint. The structural indices of beam included tension and

Table 1. Database of investigated buildings

No.	Code Name Building	Type of Story	Number Height(m)	Clear Story Length (m)	Span	Column size Tributary Area ( m <sup>2</sup> )	Approximate	Remark
1	9UNI-1	University	9	4.0	8.0	600x800	48.0	JL
2	9UNI-2	University	9	4.2	7.0	800x800	57.0	JL
3	21OFF-3	Office	21	4.5	9.0	1200x1200	40.5	JL
4	12Hos-4	Hospital	12	4.5	5.0	600x600	29.5	JM
5	12AP-5	Apartment	12	3.0	8.0	400x1200	32.4	JM
6	9SCL-6	School	9	4.0	7.0	500x800	24.0	JM
7	15AP-7	Apartment	15	3.2	4.3	400x800	20.0	JM
8	12OFF-8	Office	12	4.5	6.2	700x700	17.5	JS
9	9Ap-9	Apartment	9	2.7	3.0	200x400	9.0	JS
10	9AP-10	Apartment	9	2.5	3.4	300x500	13.7	JS



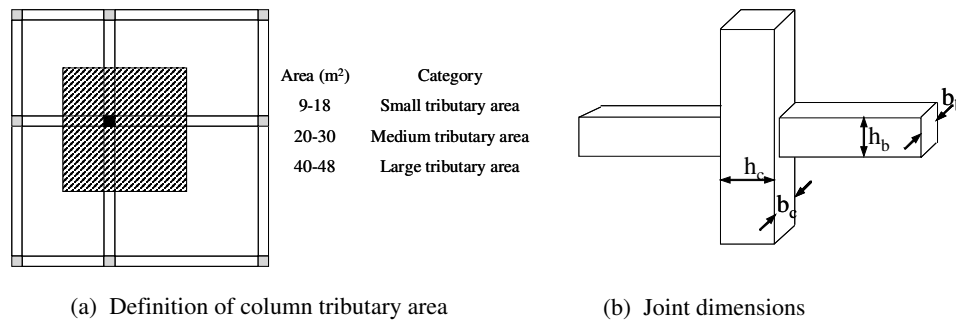


Figure 2. Definition of column tributary area and joint dimensions

compression reinforcement ratio, shear span-to-depth ratio, flexural capacity-to-shear capacity ratio, and transverse reinforcement ratio. The structural and geometrical indices of column included axial force ratio, shear span-to-depth ratio, flexural capacity-to-shear capacity ratio, longitudinal reinforcement ratio, and transverse reinforcement ratio. The structural and geometrical indices of beam-column joint included column depth-to-bar diameter ratio, column width-to-beam width ratio, column depth-to-beam depth ratio, confinement reinforcement index, column flexural capacity-to-beam flexural capacity ratio, and joint shear-to-joint shear strength ratio. Figure 2(b) illustrates the definition of joint dimensions used to calculate these indices.

The structural and geometrical indices were calculated for the beam-column joint of buildings in each category. The range of indices is shown in Table 2-4. It is noted that none of buildings had stirrups in the joint. The column longitudinal bars were usually spliced just above the joint with lap length of 350 mm. It is noted that almost all buildings had column stronger than beam. This complies with the strong column weak beam concept despite no capacity design was applied in the design of these buildings. The ratio of column depth to bar diameter ratio ( $h_c/d_b$ ) of all buildings were greater than 20, which was the minimum requirement of the ACI code (2005) for frames in high seismic zones. The significant feature is the size of column, which depends on the column tributary area. There is a tendency of increasing column size with increasing tributary area. As the column size gets larger, the bond demand represented by the bond index ( $BI = f_y d_b / 2h_c \sqrt{f'_c}$ ) of the longitudinal bar decreased, the joint shear to joint shear capacity ratio is lowered, and the nominal column to beam moment capacity increased.

### 3. Test specimens

Based on the investigated structural and geometrical indices, three half-sized beam-column specimens, namely, JL, JM, and JS were constructed to represent buildings with large, medium, and small column tributary area, respectively. The indices of these specimens were designed to be as close as possible to the mean values calculated from the actual building in each category as shown in Table 2-4. The speci-

men dimensions and reinforcement details are illustrated in Figures 3-4. The size of the column in the direction of loading is 400, 350, and 300 mm, respectively. However, the beam depth was kept constant in all three specimens to keep the ratio of beam height to column height close to the collected data as shown in Table 2-4. The 12-mm diameter reinforcing bar was used as a longitudinal reinforcement in beam and column. The average tested yield and tensile strengths of the bar were 499 and 615 MPa, respectively. The 3-mm diameter plain mild steel bar was used as a transverse reinforcement in beam and column. The tested yield and tensile strengths of the bar were 291 and 339 MPa, respectively. The average tested compressive strength of a standard concrete cylinder at 28 days was 26.7 MPa.

### 4. Test set-up and boundary condition

The test set-up and boundary conditions are shown in Figure 5. The lateral forced displacement was applied at the top of the column through a 500 kN hydraulic actuator. The ends of the beam were supported by rollers that allowed free horizontal movement to simulate lateral drift. The bottom end of the column was supported by a hinge which allowed no movement in any direction. The axial load of

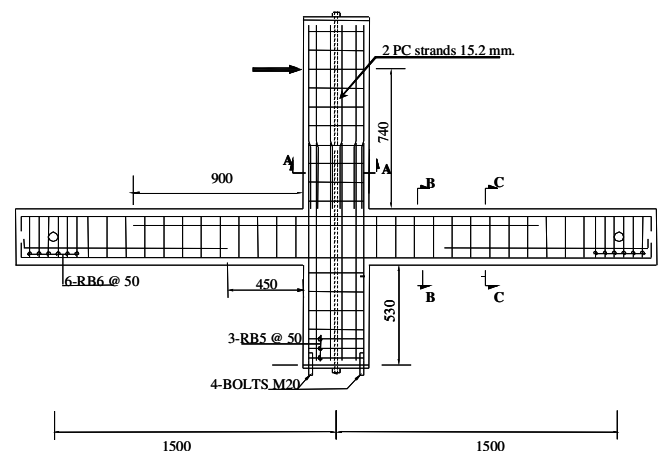


Figure 3. Geometry, dimension and reinforcement of all specimens (unit:mm)

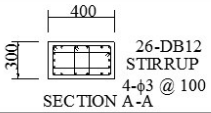
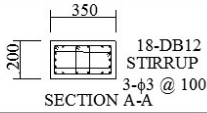
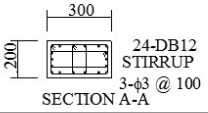
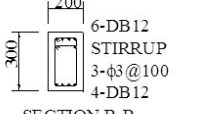
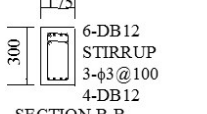
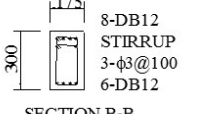


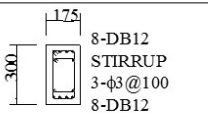
Member detail	JL-specimen	JM-specimen	JS-specimen
Column detail			
Beam detail			
			

Figure 4. Cross section of beams and columns (unit: mm)

Table 2. Structural indices for buildings with large tributary area

No.	Code	Clear story Height (m)	BI		$\frac{b_b}{b_c}$	$\frac{h_b}{h_c}$	$\frac{M_{nc}}{M_{nb}}$	$\frac{V}{V_n}$	$\frac{\rho_{sv} f_y}{f'_c}$
1	9UNI-1	4.0	4.30	32	0.417	0.750	3.442	1.126	0.0
9	9UNI-2	4.2	4.81	29	0.625	1.000	2.098	0.972	0.0
10	21-OFF-3	4.5	3.09	48	0.417	0.667	5.047	0.911	0.0
	Maximum	4.5	4.81	48	0.625	1.000	5.047	1.126	0.0
	Minimum	4.0	3.09	29	0.417	0.667	2.098	0.911	0.0
	Average	4.2	4.07	$3\overline{d_c}$	0.486	0.806	3.529	1.003	0.0
	Std. Dev.	0.3	0.88	$10\overline{d_b}$	0.120	0.173	1.477	0.111	0.0
	Specimen JL		4.45	33	0.667	0.750	3.049	0.903	0.0

Table 3. Structural indices for buildings with medium tributary area

No.	Code	Clear story Height (m)	BI	$\frac{h_c}{d_b}$	$\frac{b_b}{b_c}$	$\frac{h_b}{h_c}$	$\frac{M_{nc}}{M_{nb}}$	$\frac{V}{V_n}$	$\frac{\rho_{sv}f_y}{f'_c}$
4	12Hos-4	4.5	6.19	24	0.500	1.083	2.372	0.912	0.0
5	12AP-5	3	2.24	60	0.750	0.667	3.403	1.029	0.0
6	9SCL-6	4	4.96	32	0.700	1.000	1.538	1.115	0.0
7	15AP-7	3.2	4.64	32	0.750	0.625	2.127	1.172	0.0
	Maximum	4.5	6.19	60	0.750	1.083	3.403	1.172	0.0
	Minimum	3.0	2.24	24	0.500	0.625	1.538	0.912	0.0
	Average	3.7	4.51	37	0.675	0.844	2.360	1.057	0.0
	Std. Dev.	0.7	1.65	16	0.119	0.232	0.779	0.113	0.0
	Specimen JM		5.09	29	0.875	0.857	1.682	1.382	0.0

12.5% of column axial capacity was applied to the column by means of vertical prestressing. The column was pushed forward and pulled backward in a reversed cyclic. The load type was quasi-static with the load application rate of half an hour to complete one cycle. The lateral drift ratio, defined as

the ratio of the lateral displacement at the top of the column to the column height, was incrementally applied at 0.25%, 0.50%, 0.75%... as shown in Figure 6. The target loop was repeated twice for each drift level. The load was continued until and beyond the peak load to trace the post-peak behav-

Table 4. Structural indices for buildings with small tributary area

No.	Code	Clear story Height (m)	BI	$\frac{h_c}{d_b}$	$\frac{b_b}{b_c}$	$\frac{h_b}{h_c}$	$\frac{M_{nc}}{M_{nb}}$	$\frac{V}{V_n}$	$\frac{\rho_{sv} f_y}{f'_c}$
8	12OFF-8	4.5	5.94	25	0.571	1.143	0.732	2.668	0.0
9	9Ap-9	2.7	5.90	25	1.000	1.000	2.331	1.677	0.0
10	9AP-10	2.5	8.57	20	0.833	0.900	1.473	3.504	0.0
	Maximum	4.5	8.57	25	1.000	1.143	2.331	3.504	0.0
	Minimum	2.5	5.90	20	0.571	0.900	0.732	1.677	0.0
	Average	3.2	6.80	23	0.802	1.014	1.512	2.616	0.0
	Std. Dev.	1.1	1.53	3	0.216	0.122	0.800	0.915	0.0
	Specimen JS		5.94	25	0.875	1.000	1.187	2.282	0.0

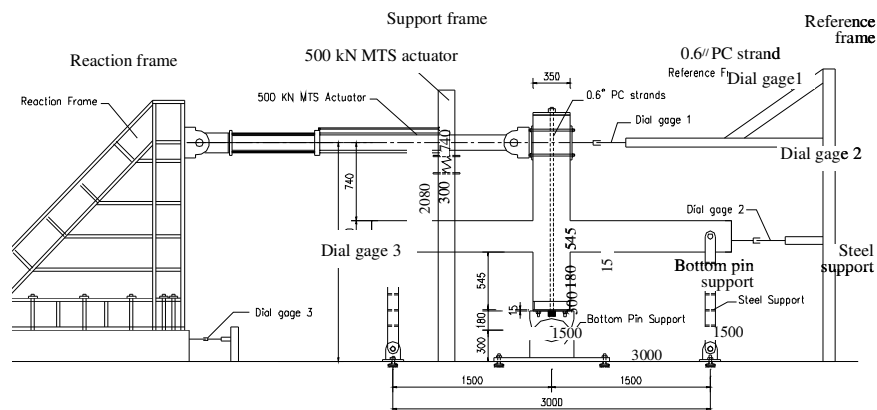


Figure 5. Test set-up

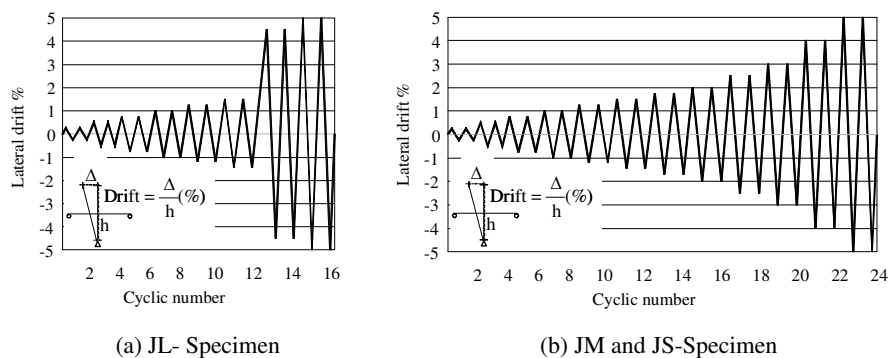


Figure 6. Displacement history of each specimen

ior. The measurements included forces, displacements, and strains at various locations of the specimens.

## 5. Test Results and Discussions

### 5.1 General observation, cracking process and failure mode

Specimen JL showed first flexural cracks in the beam during 0-0.25% drift ratio. The behavior was elastic during

these initial drifts as shown in Figure 7(a). The flexural cracks grew in size and number as the drift ratio increased. The beam yielded at 1.0% drift. The first diagonal crack at the joint was observed at 1.25% drift. Bond splitting cracks were also observed at the longitudinal steel level. The beam maintained yielding up to 4.6% drift when substantial crushing of concrete at the beam compression zone took place and spalled off, exposing beam bars as shown in Figure 8(a). The specimen lost its strength abruptly. Throughout the entire loading, no cracks were observed in the column lap

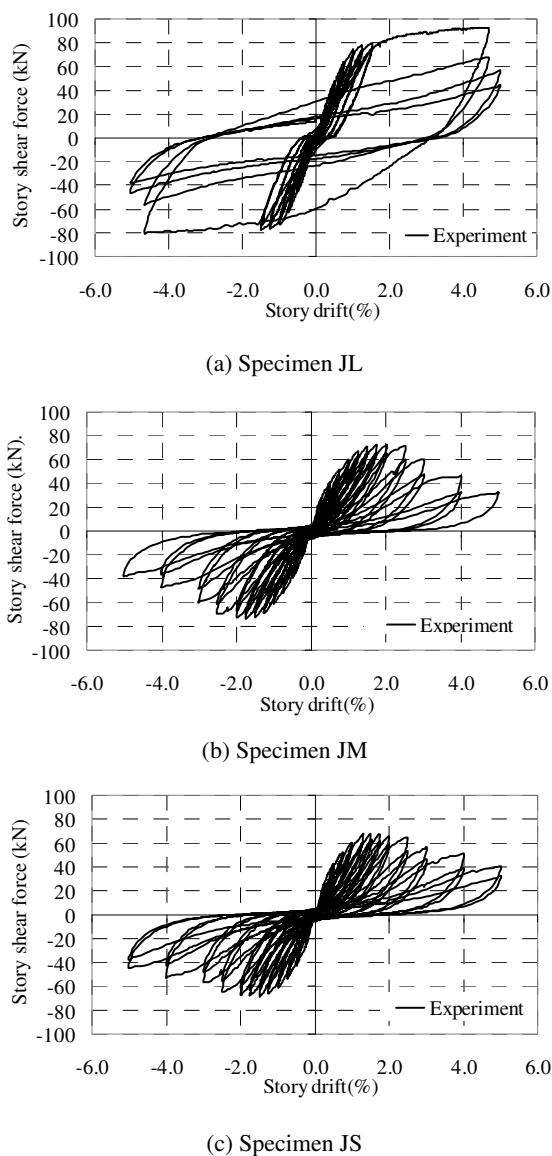


Figure 7. Relationship between applied load and displacement of each specimen

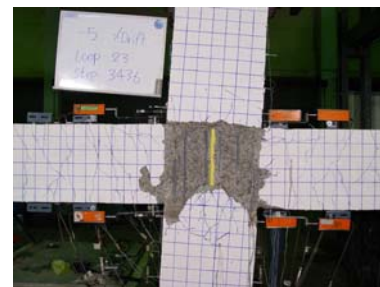
splice region above the joint. No damage was observed in the joint except some few joint shear cracks. The failure of the beam was classified as ductile flexural failure. The hysteresis loops were wide, indicating large energy dissipation in bending mode. It is noted that even though the specimen lacked ductile reinforcement details and was not designed to resist seismic load, it could perform fairly well. The good performance was supposedly attributed to the size of column which was comparatively large, in order to support large gravity load for the large tributary area. As the column size is large, the joint shear stress has decreased naturally, and the bond demand of the column lap splice is relieved. The bending failure then occurred in the beam according to strong column weak beam principle. This experiment demonstrated that the performance of beam-column joint was

satisfactory, when the column size was large even without ductile reinforcement details. However, the ductility can be enhanced by providing closed stirrups near the beam s end to prevent concrete spalling and reinforcement buckling.

The behavior of JM and JS was similar, hence they are discussed together. The flexural cracks were observed in the beam in the beginning of the 0-0.25% drift ratio (Figures 7(b), 7(c)). The first diagonal crack was found in the joint core at 0.5% drift ratio. They formed an X-pattern following the alternate load directions. The flexural cracks in beams and the diagonal cracks in joint cores continued to grow in size and number until the specimen reached the peak load of 72 kN at 1.75% drift ratio for specimen JM, and 68 kN at 1.5% drift ratio for specimen JS. After this cycle, no new cracks were found in the beam, but diagonal cracks continued to widen in the joint core. This was followed by spalling of concrete at the center of the joint area. At 3% drift, the concrete spalling extended throughout a wider area of the joint, exposing column longitudinal bars. The test was continued until 5% drift ratio, where concrete spalling covered



(a) Failure of specimen JL



(b) Failure of specimen JM



(c) Failure of specimen JS

Figure 8. Failure of specimen

the entire joint area (Figures 8(b), 8(c)) and extended into the column above and below the joint. The failure mode of JM and JS could be classified as joint shear failure. It should be noted that no damage was observed at the column bar splice region above the joint. The joint shear failure is not desirable as it is abrupt and results in pinched hysteresis loops with low energy dissipation. The experiment indicated the vulnerability of existing buildings with small column tributary area. Future research should look into the retrofiting of these classes of buildings.

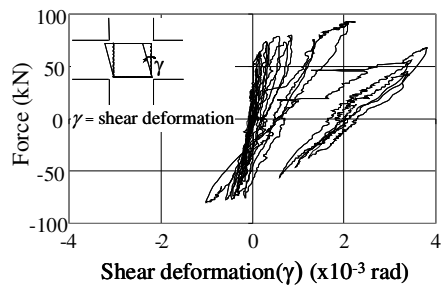
## 5.2 Force-joint shear deformation relation

To gain an insight into the behavior of each specimen, local deformations and strains were measured at critical regions of the specimens. The force-shear deformation in the joint zone is compared among three specimens in Figure 9. The joint shear deformation was plotted in terms of shear angle. Specimen JL showed clearly smaller joint shear de-

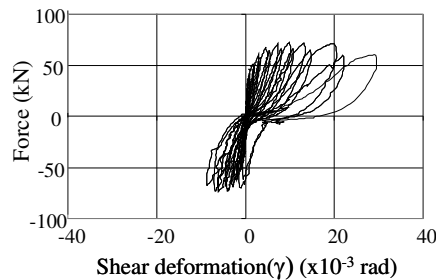
formation compared with JM and JS. The maximum values of shear deformation at failure were 0.00012, 0.02 and 0.015 radian in JL, JM and JS, respectively. These shear deformation values correlated well with observed damage level in the joint of each specimen. Little shear inelasticity was observed in JL, while substantial damage existed in joints of specimen JM and JS. On the other hand, the hysteresis force versus shear deformation of JM and JS showed severe pinching, which partly accounted for the pinching of the global load displacement relation.

## 6. Force-steel strain relation

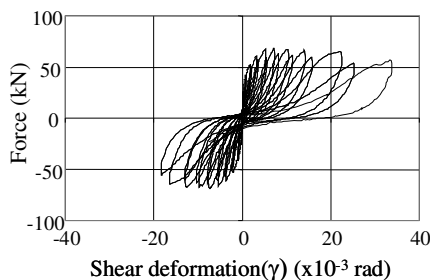
The force and strain relations of bottom bars located 50 mm away from the joint face (STBBR-gage) and at the middle of the joint (STBBM-gage) are plotted in Figures 10 and 11. Specimen JL reached yielding and developed large plastic strain, while JM and JS merely reached yielding without developing high plasticity. In each specimen, the



(a) Specimen JL

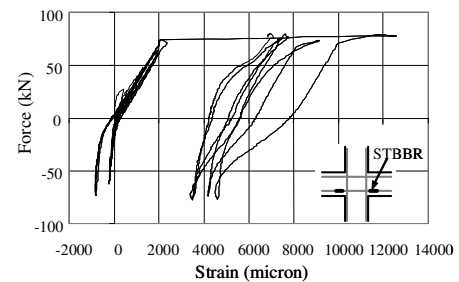


(b) Specimen JM

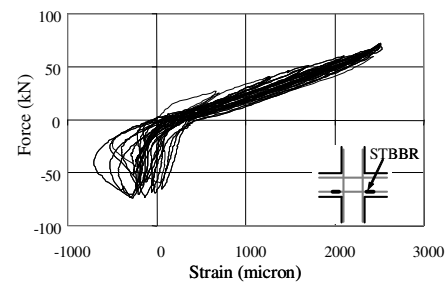


(c) Specimen JS

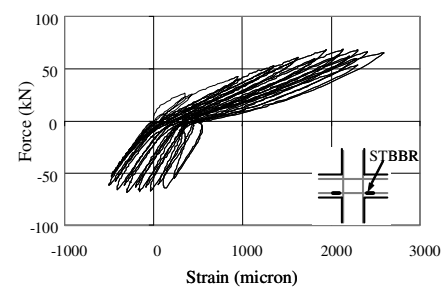
Figure 9. Force- joint shear deformation relationship of each specimen



(a) Specimen JL



(b) Specimen JM



(c) Specimen JS

Figure 10. Strain of bottom beam bar (STBBR) at 50 mm away from the joint face



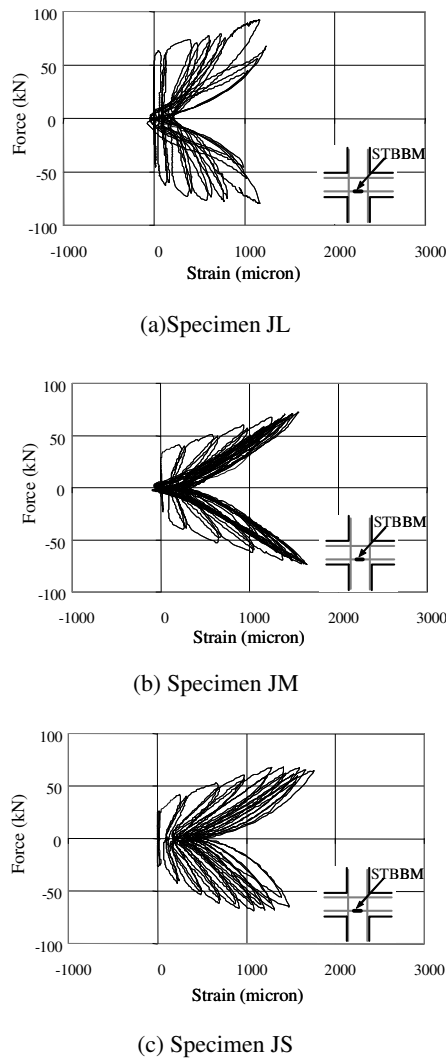


Figure 11. Strain of bottom beam bar (STBBM) at the middle of joint

strains of bottom beam bars at 50 mm from the joint face and at the middle of the joint showed obviously different behaviors. At 50 mm from the joint face, the steel bar of JL was subject to alternate compressive and tensile strains in the early drift levels. But the strains turned into purely tensile at high drift levels regardless of the loading direction. As for JM and JS, the strain behavior on the tensile and compressive sides was obviously unsymmetrical. This is due to the fact that the strain of the steel bar was smaller on the compressive than on the tensile side. With increasing drift ratio, the tensile strain continuously increased, whereas the compressive strain (negative strain value) initially increased, but gradually decreased later. This behavior was dealt with by the interface pull-out crack, which was caused by local bond deterioration, and had taken place in the previous opposite load direction. During reverse loading, the pull-out crack was not completely closed, thus, a positive strain value still remained in steel, and was accumulated in subsequent cycles. The steel on the compression side became positive instead

of negative.

The behavior of the steel bar at the middle of the joint showed a butterfly pattern. The strains on the compression and tension side were symmetrical at about zero force level. The steel strain at the middle of the joint of all specimens was always tensile regardless of the load direction. Furthermore, it should be noted that strains at the middle of the joint were approximately equal in all specimens, and that the magnitude was less than the yield strain. As seen for all specimens, the yielding did not spread deep into middle of the joint. This was contrasted with the value at 50 mm away the column face, especially for the steel strain in JL. This indicated that the bond within joint core was not completely lost along the length of the bar. The variations of strain with load cycles are plotted in Figures 12(a)-12(c). Specimen JL maintained bond conditions quite well before yielding at 1.25% drift ratio. After yielding, the bar strain was purely tensile, indicating the local loss of bond at the section with high strain value. For Specimen JM and JS, the local bond was lost in the early 0.75% drift.

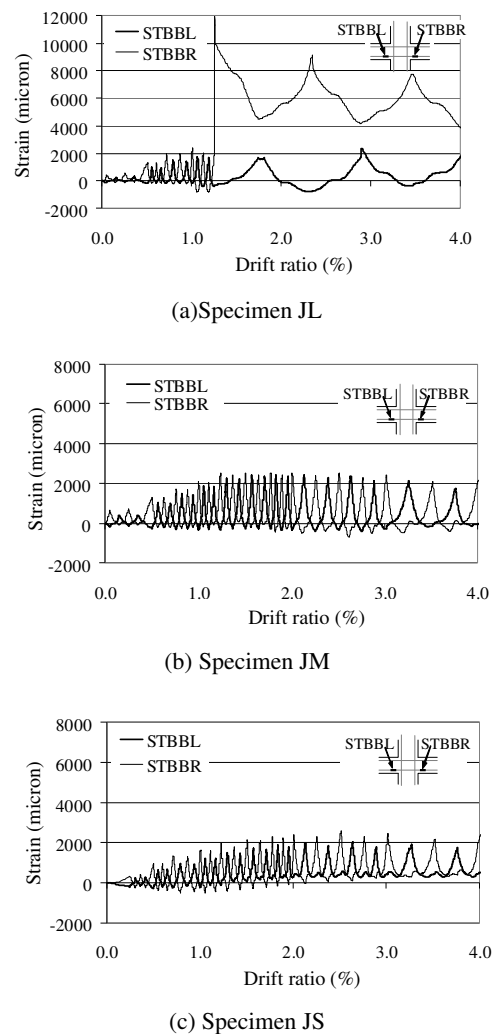


Figure 12. Strain history of bottom beam bar at 50 mm away from the joint fac

The bond demand of longitudinal beam bar was associated with the ratio of column depth to bar diameter ( $h_c/d_b$ ). According to the ACI code, this ratio is required to be not lower than 20 for frames in high seismic zones. The  $h_c/d_b$  ratios of JL, JM, and JS were 33, 29, and 25, respectively. Therefore, the bond demand of JS seemed to be more severe than of JM and JL, because the size of the column was smaller. In view of the experimental results, no entire loss of bond was observed in any specimen. But, the local loss of bond at the beam section close to the joint could not be avoided in all specimens. This local bond loss was associated with pull-out slip of beam bars.

## 7. Conclusion

This paper presented the reversed cyclic test of non-ductile designed interior RC beam-column joints typical for constructions in low to moderate seismic zones. According to the evaluation of ten old existing RC beam-column frame buildings, there existed some correlations among key structural and geometrical indices and the column tributary area. With increasing tributary area, the trend indicated larger column size, lower bond demand, lower joint shear stress, and higher column flexural capacity. The experimental results showed that specimens with small to medium column tributary area were vulnerable to brittle joint shear failure, while specimen with large column tributary area could achieve moderately ductile yielding, even though the ductile reinforcement detailing was not provided. The strain measurements of longitudinal steels indicated local bond deterioration of steel bars at the column face in all specimens, but the bond deterioration did not spread in to the center of the joint core. No entire loss of bond was observed in all specimens. But the local bond pull-out was observed in all specimens, although all satisfied the minimum ACI column depth to bar diameter ratio of 20. The source of severe pinching in hysteresis loops was derived from the bond pull-out and joint shear distress.

## Acknowledgements

The authors are very grateful to the Thailand Research Fund (TRF) for providing the research fund RMU4880022 to carry out the research.

## References

- ACI committee 318. 2005. Building Code Requirements for Structural Concrete and Commentary, Michigan
- Aycardi, L.E., Mander, J.B. and Reinhorn, A.M. 1994. Seismic resistance of reinforced concrete frame structure designed only for gravity loads: Experimental performance of subassemblages, *ACI Structural Journal*, 91(5): 552-563
- Bracci, J.M., Reinhorn, A.M. and Mander, J.B. 1995. Seismic resistance of reinforced concrete frame structure designed only for gravity loads: Performance of Structure system, *ACI Structural Journal*, 92(5): 597-609
- CEB State of the Art Report. 1996. RC frames under earthquake loading, Thomas Telford, London
- El-attar, A.G., White, R.N., and Gergeley, P. 1997. Behavior of gravity load designed reinforced concrete buildings subjected to earthquakes, *ACI Structural Journal*, 94(2):133-145.
- Hakuto, S., Park, R., and Tanaka, H. 2000. Seismic load tests on interior and exterior beam-column joints with substandard reinforcing details, *ACI Structural Journal*, 97(1): 11-25.
- Hegger, J., Sherif, A. and Roeser, W. 2003. Nonseismic design of beam-column joint. *ACI Structural Journal*, 100(5): 654-664.
- Li, B. and Pan, T.C. 2004. Seismic performance of reinforced concrete frames under low intensity earthquake effects, *Proceedings of the 13<sup>th</sup> World Conference on Earthquake Engineering*, Vancouver
- Li, B., Wu, Y. and Pan, T.C. 2002. Seismic behavior of non-seismically detailed interior wide beam-column joints-Part I: Experimental results and observed behaviors, *ACI Structural Journal*, 99(6): 791-802.
- Maekawa, K., Pimanmas, A. and Okamura, H. 2003. Non-linear mechanics of reinforced concrete, Spon Press, London.
- Park, R. 2002. A Summary of Results of Simulated Seismic Load Tests on Reinforced Concrete Beam-Column Joints, Beams and Columns with Substandard Reinforcing Details. *Journal of Earthquake Engineering*, No 6: 147-174
- Riggs, H., and Powell, G. 1986. Rough crack model for analysis of concrete, *ASCE J. Eng. Mech*, 112(5): 448-464
- Supaviriyakit, T., Pimanmas, A. and Warnitchai, P. 2006. Effect of removing initial bond between beam bar and concrete on cyclic response of non-ductile beam-column joint, *Proceeding of 10<sup>th</sup> East Asia-Pacific Conference on Structural engineering and construction*, Thailand.
- Vecchio, F.J., and Collins, M.P. 1986. The modified compression field theory for reinforced concrete elements subjected to shear, *ACI Structural Journal*, 83(2): 219-231.
- Vecchio, F.J., and Collins, M.P. 1988. Predicting the response of reinforced concrete beams subjected to shear using the modified compression field theory, *ACI Structural Journal*, 85(4): 258-268.
- Warnitchai, P. 2004. Development of seismic design requirements for buildings in Bangkok against the effects of distant large earthquakes, *Proceedings of the 13<sup>th</sup> World Conference on Earthquake Engineering*, Vancouver

**Notation**

		$f_y$	yield strength of reinforcement
$b_b$	beam width	$M_{nc}$	nominal column flexural capacity
$b_c$	column width	$M_{nb}$	nominal beam flexural capacity
$d_b$	diameter of longitudinal beam bar	$V$	joint shear force
$h_b$	beam depth	$V_n$	joint shear strength
$h_c$	column depth	$\rho_{sv}$	volumetric ratio of confinement reinforcement
$E_s$	elastic modulus of steel bar	BI	bond index ( $BI = f_y d_b / 2h_c \sqrt{f'_c}$ )
$f'_c$	cylindrical compressive strength of concrete		

## Assessment of Seismic Deficiency of Existing Reinforced Concrete Buildings in Bangkok

Panuwat Joyklad<sup>1</sup>, Preeda Chaimahawan<sup>2</sup> and Amorn Pimanmas<sup>2</sup>

Sirindhorn International Institute of Technology, Thammasat University

PO Box 22, Thammasat-Rangsit Post Office

Pathumthani 12121, Thailand

Tel: 0-2986-9009 Ext. 2403, Fax: 0-2986-9009 Ext. 1900

E-mail: <sup>1</sup>joy.civil@gmail.com, <sup>2</sup>preeda\_sj@hotmail.com, <sup>2</sup>amorn@siit.tu.ac.th

### Abstract

This paper presents a result of assessment of seismic deficiency of buildings in Bangkok. The target buildings are mid-rise reinforced concrete beam-column frames having 5-15 stories. The occupancy type is essential and assembly facilities including schools, university, governmental offices and apartments. Many of these buildings with more than 6 stories are usually provided with reinforced concrete lift core. The seismic evaluation methodology consists of demand to capacity ratio determination (DCR), reinforcement detailing check and failure mode investigation. Eight buildings are examined. The seismic deficiency is checked against earthquake loading specified in No.49 Ministerial Law [1] and the ACI [2] requirements for Intermediate Moment Resisting Frame. The region of interest is the first floor sub-frame where the lateral shear is supposed to be highest. The moment frames in both transverse and longitudinal directions are considered. The result shows that all eight buildings do not satisfy reinforcement detailing criteria. Five out of eight buildings do not satisfy DCR criteria. Based on the failure mode investigation, the result shows 44% of beam flexural failure, 41% of joint shear failure and 15% of beam shear failure. It is seen that shear failure covers 66% of the total. The majority of failure is found in beams. The reason why the DCR criteria is not critical is due to traditional working stress design approach for RC structures in Thailand with lower allowable compressive strength of concrete and steel compared to more modern ultimate strength design codes. Another reason is the presence of

lift core that reduces the forces transmitted to beam-column frame.

### 1. Introduction

Although Bangkok, the capital city of Thailand is not directly located on fault, it is not safe from distant earthquakes. On 26<sup>th</sup> December 2004, the Sumatra earthquake of 9.3 magnitude on Richter scale has caused a devastating Tsunami and hit the coast of Thailand with more than 5,000 lost of lives. In that event, though approximately 800 km away from Bangkok, many high rises in Bangkok were severely shaken. This caused a widespread public concern on the safety of building in seismic events.

Bangkok is vulnerable to earthquake because the city is founded on soft marine clay which can amplify earthquake up to three to four times [3]. Moreover, almost all buildings in Bangkok have not been traditionally designed against seismic loading. In order to mitigate the possible seismic hazard, buildings should be evaluated for seismic rating and necessary preparedness is required, especially public buildings such as academic buildings, apartment buildings, governmental buildings and hospital should be able to withstand earthquake as they are supposed to provide post earthquake rescue operation.

A study on seismic evaluation of RC buildings in Bangkok is presented in this paper. In this study, existing reinforced concrete buildings constructed as beam-column frames are investigated to identify the typical characteristics of building designed for gravity load only, especially the reinforcement detailing. This study focuses on reinforced concrete frames having 5-15 stories. According